Chapter 5

Results

In this chapter, we present results for the equilibrium and nonequilibrium magnetic behavior of laterally nanostructured films during growth. We apply the bilayer island growth mode as a model system. Results on the magnetic ordering, the magnetic relaxation from the saturated state, and on the magnetic domain structure during film growth are shown and discussed in detail. For these investigations, the film magnetization, the average magnetic domain area, and the domain roughness are calculated as functions of film coverage Θ, temperature T, and MC time t. The influence of the irregular nanostructure and the magnetic interactions is studied.

First, in **Sec. 5.1**, the calculated quantities and magnetic parameters are defined. Next, in **Sec. 5.2**, we demonstrate the improved relaxation behavior of the CSF algorithm in comparison to the SSF algorithm for irregularly connected film structures when starting from the aligned island spin state. In **Sec. 5.3**, we show results for the long-range magnetic ordering. The influence of the island-island interactions for film coverages below and above the percolation threshold Θ_{P} is studied. For this purpose, we use the equilibrium MC method. The MC results are compared to results obtained by use of a simple mean-field theory. The validity of this simple method is discussed. In **Sec. 5.4**, we turn to results for the magnetic relaxation from the aligned island spin state, obtained by the kinetic MC method. We study the influence of the magnetic interactions in the entire coverage range. Finally, in **Sec. 5.5**, we present results on the metastable 'as-grown' magnetic domain structure during film growth which are obtained by use of the kinetic MC method. Here, we start the simulations from random island spin states, the temporal developement of the atomic and magnetic structure happens simultaneously.

5.1 Calculated quantities and parameters

In the present thesis, the bilayer island growth mode, see Sec. 2.2.2, is used as a model system of a growing island-type film. After a particular realization of this growth mode at coverage Θ has been performed, the mutual distances between the island centers r_{ij}, the nonuniform distributions of island sizes $N_i(\Theta)$, the number of atomic bonds $L_{ij}(\Theta)$ between connected islands, and the average atomic coordination numbers of the islands $\overline{q}_i(\Theta)$ are analysed. These quantities provide the structural input for the magnetic calculations.

In Secs. 5.2, 5.3, and 5.4, results for the **remanent magnetization** $M_{\rm rem}$ and the **equlibrium magnetization** $M_{\rm eq}$ of growing film systems are presented as functions of film coverage Θ, temperature T, and MC time t. Here, the MC simulations always start from the fully aligned island spin state $\boldsymbol{X}_1 = \{+1, \ldots, +1\}$. The choice of this initial state mimics experiments which saturate the magnetic system by an external magnetic field, and determine the remanent magnetization after removal of the field [47, 151, 17]. $M_{\rm eq}$ is determined according to Eqs. (4.6), (4.8), and (4.9) and is obtained by averaging over at least $(t_3 - t_2) = 1000$ MCS (MC steps/spin) after the system has become equlibrated. $M_{\rm rem}$ is calculated by use of Eqs. (4.6), (4.11), and (4.9). Both magnetizations are averaged over at least $G = 20$ different structural runs. $M_{\rm eq}$ and $M_{\rm rem}$ are given in units of a saturated monolayer ($\Theta = 1$ ML) at $T = 0$.

We point out that for certain simulation parameters the finite-sized unit cell occasionally undergoes total magnetic reversals during MC probing, since the applied algorithms are fully ergodic. This can lead to unintended cancellations of finite magnetization components $M_{\rm rem}$ and $M_{\rm eq}$ with opposite signs during structural and temporal averaging. To avoid this, we average over the *absolute* values $|M_{\rm rem}|$ and $|M_{\rm eq}|$.

For the island spin flip probabilities per MC step (Eq. (4.12)), we apply the prefactor $\kappa = 0.1$. Thus, in kinetic simulations a MC time step $\Delta t = 1$ MCS refers to the physical time step $\Delta t' = \kappa\, \Delta t = 0.1$ sec.

The results on the magnetic domain structure during film growth, presented in Sec. 5.5, are obtained by the kinetic MC method. Here, film growth and magnetic relaxation evolve simultaneously. The following simulation procedure is applied: First, island seeds with random spin directions are distributed over the unit cell. Thus, the initial island spin states $\boldsymbol{X}_1 = \{S_1, \ldots, S_Z\}$ refer to *random* states in phase space. The film growth up to a coverage $\Theta = 2$ ML is divided into 400 growth steps. After each growth step, the quantities $N_i(\Theta)$, $L_{ij}(\Theta)$, and $\overline{q}_i(\Theta)$, resulting from the growth procedure, are determined, and the magnetic structure of the island ensemble is allowed to relax towards its thermal equilibrium, applying $t = 100$ MCS. This procedure is repeated until the desired film coverage is obtained. For the connection to a physical time unit, we apply the prefactor $\kappa = 0.005$

	I	II
γ [meV]	5.6	5.8
J [meV]	7.0	7.3
K_1 [meV]	0.01	0.2
K_2 [meV]	0.1	
μ_{at} [μ_{B}]	2.0	

Table 5.1: Magnetic parameters used in the MC calculations. J is the exchange integral between atomic spins, γ is the domain wall energy or inter-island exchange coupling, K is the effective anisotropy constant, and μ_{at} is the atomic magnetic moment in units of Bohr magneton. We apply different parameter sets I and II.

in Eq. (4.12). Thus, the adatom deposition rate of the film is adjusted to 1 ML/100 sec which is a typical experimental value [17, 3]. In addition, we present results for a deposition rate of 1 ML/10000 sec, which is adjusted by the same prefactor κ and $t = 10000$ MCS for the magnetic relaxation in each growth step.

The 'as-grown' magnetic domain structure is analysed by identifying connected islands with a parallel magnetization as a magnetic domain. For this purpose, the Hoshen-Kopelman algorithm [68] is used, see Appendix C. Only the first magnetic layer is analysed for the determination of the number of domains in a single MC run and the **domain areas** A_i in units of lattice sites. Additionally, the **domain roughnesses** R_i are calculated by use of the definition

$$R_i \equiv \partial A_i / A_i \quad , \tag{5.1}$$

where ∂A_i is the number of atomic magnetic moments at the outer edge of a domain. Since for a domain with an increasing area, its edge-to-area ratio is always decreasing, we consider here the *relative* domain roughness

$$r_i = R_i / R_i^{\circ} \tag{5.2}$$

with respect to the minimal roughness (smallest possible edge-to-area-ratio) $R_i^{\circ} \propto \sqrt{A_i}$ of a circularly shaped domain with the same area A_i. In this study, we present results for the *mean* values $\overline{A}(\Theta, T)$ and $\overline{r}(\Theta, T)$ as functions of film coverage Θ and temperature T which are obtained by averaging over all domains of a single MC run and over at least 20 MC runs for film growth and magnetic relaxation.

In the remainder of this section, we specify the **magnetic and structural parameters**. Growing thin films are characterized by a large amount of nonequivalent lattice sites, corresponding to a large number of different interaction parameters. Since little is known about these values, we use averaged quantities for the magnetic parameters which are fixed as shown in

Tab. 5.1, using mainly as an example the Co/Cu(001) thin film system. Two different sets of parameters are applied for our calculations.

For the results of Secs. 5.2, 5.3, and 5.4, parameter set I is used in connection with version I of the bilayer island growth mode, see Tab. 2.1, p. 29. The *inter*-island exchange coupling (domain wall energy) γ is adjusted to result in a Curie temperature $T_\mathrm{C} = 355$ K of the *long-range* ferromagnetic order at $\Theta = 2$ ML which was measured for a 2-ML Co/Cu(001) film [17]. We obtain $\gamma = 5.6$ meV. In a laterally nanostructured film, consisting of partly connected islands, the *internal* ordering temperature of the islands $T_\mathrm{C}^\mathrm{int}$ is larger than T_C. Due to the lack of measurements for $T_\mathrm{C}^\mathrm{int}$, the exchange integral J is chosen to yield $T_\mathrm{C}^\mathrm{int}(2\,\mathrm{ML}) = 430$ K within the mean-field theory, given in Appendix F.1. This results in $J = 7.0$ meV. We point out that on one hand this value is somewhat arbitrary, but on the other hand, the results of this study depend only weakly on the exact value of J. For the uniaxial anisotropy constatnt, we use the typical value $K_1 = 0.01$ meV, measured for thin Co/Cu(001) films [60, 91], and the value $K_2 = 0.1$ meV, to consider the effect of a larger anisotropy which is often found in low-dimensional systems [15, 2, 134]. The atomic magnetic moments are set to $\mu_\mathrm{at} = 2.0\,\mu_\mathrm{B}$, as measured for 2-ML Co/Cu(001) films [155].

For the calculations of the magnetic domains, the magnetic parameters of set II together with version II of the bilayer island growth mode are applied. These parameters are adjusted to $T_\mathrm{C}(2\,\mathrm{ML}) = 355$ K and $T_\mathrm{C}^\mathrm{int}(2\,\mathrm{ML}) = 450$ K. For the anisotropy constatnt, the value $K_1 = 0.2$ meV is used, resulting from measurements on thin Co/Au(111) films [2].

5.2 Test of the cluster Monte Carlo method

In this section, we compare the relaxation behavior resulting from the conventional single-spin-flip (SSF) and from the newly developed cluster-spin-flip (CSF) MC algorithm, described in Secs. 4.2.1 and 4.2.2. We show results for the relaxation of the remanent magnetization $|M_\mathrm{rem}^0(\Theta, T, t)|$ in the MC process towards thermodynamical equilibrium for coverages Θ below and above the percolation threshold $\Theta_\mathrm{P} = 0.9$ ML of the bilayer island growth mode. For this comparison, exclusively the inter-island exchange coupling with $\gamma = 5.6$ meV is considered, the dipole interaction as well as single-island anisotropy barriers are neglected. The relaxation of the remanent magnetization is calculated as described in Sec. 4.1.2. Solely Metropolis-type flip rates (Eq. (3.39)) are used. The MC process is always started from a fully aligned island spin state $\boldsymbol{X}_1$.

First, we test for an almost homogeneous film, whether by use of the CSF method the remanent magnetization $|M_\mathrm{rem}^0|$ relaxes into the correct equilibrium value $|M_\mathrm{eq}^0|$. We expect that this important prerequisite is satisfied by

CSF, since it obeys detailed balance and ergodicity, as shown in Sec. 4.2.2. The strongly connected film structure can be treated by the SSF method, since here the inter-island couplings are almost uniform.

Fig. 5.1 (a) shows the remanent magnetization $|M^0_{\rm rem}(\Theta, T, t)|$ as function of MC time (MC steps) t for temperature $T = 300$ K and coverage $\Theta = 1.8\,{\rm ML} \gg \Theta_{\rm P} = 0.9$ ML, see Fig. 2.6 (i), p. 30. Since the finite-sized unit cell occasionally undergoes total magnetic reversals during MC probing, which is facilitated by CSF, in the present study we average over the absolute values of the magnetization component. We observe that by use of CSF, applying different maximum numbers $\lambda_{\rm max}$ of island spins probed for coherent rotations, $|M^0_{\rm rem}|$ relaxes into the same stable value $|M^0_{\rm eq}(\Theta, T|$, as obtained by SSF. This finite magnetization indicates the long-range ferromagnetic order of the connected system. The relaxation is slower for larger $\lambda_{\rm max}$. This property is due to the fact that for the assumed temperature the magnetic relaxation is mainly provided by flips of single spins, which are still included in CSF, or small spin clusters. As mentioned in Sec. 4.2.2, no additional relaxation channels are opened by use of CSF. Hence, the number of single-spin-flip attempts becomes reduced in favor of unprobable cluster-flip ones.

In this figure, as well as in the forthcoming ones, examples for the statistical errors are given, which result from the different averaging procedures (thermal fluctuations and different structural realizations of the unit cell). The size of the errorbars can be reduced by use of a larger unit cell, since the nonuniform system is self-averaging.

In Fig. 5.1 (b), we demonstrate that CSF achieves the correct equilibrium magnetization, as obtained by SSF, in the entire temperature range at coverage $\Theta = 1.8$ ML. The equilibrium magnetization $|M^0_{\rm eq}(\Theta, T)|$ is shown as function of temperature T. The different symbols refer to the two MC algorithms. We have used $\lambda_{\rm max} = 100$ for CSF. Excellent agreement between the two methods is obtained. We conclude that by use of the CSF algorithm correct equilibrium magnetizations are obtained for well connected film structures.

Next, we demonstrate that the main improvement of CSF with respect to SSF is obtained for film coverages Θ which are characterized by a considerable amount of island cluster formation, and hence, very irregular inter-island exchange couplings γ_{ij}. Generally, such systems are very difficult to be studied analytically.

In Fig. 5.2 (a), the remanent magnetization $|M^0_{\rm rem}(\Theta, T, t)|$ is depicted as function of MC time (MC steps) t for coverage $\Theta = 0.8$ ML, shortly below the percolation threshold $\Theta_{\rm P} = 0.9$ ML, see Fig. 2.6 (d), p. 30. Results for SSF and CSF, using different maximum spin cluster sizes $\lambda_{\rm max}$, are plotted for temperature $T = 30$ K. The equilibrium magnetization $|M^0_{\rm eq}(\Theta, T)|$ should vanish for nonpercolated systems, since no long-range interactions are

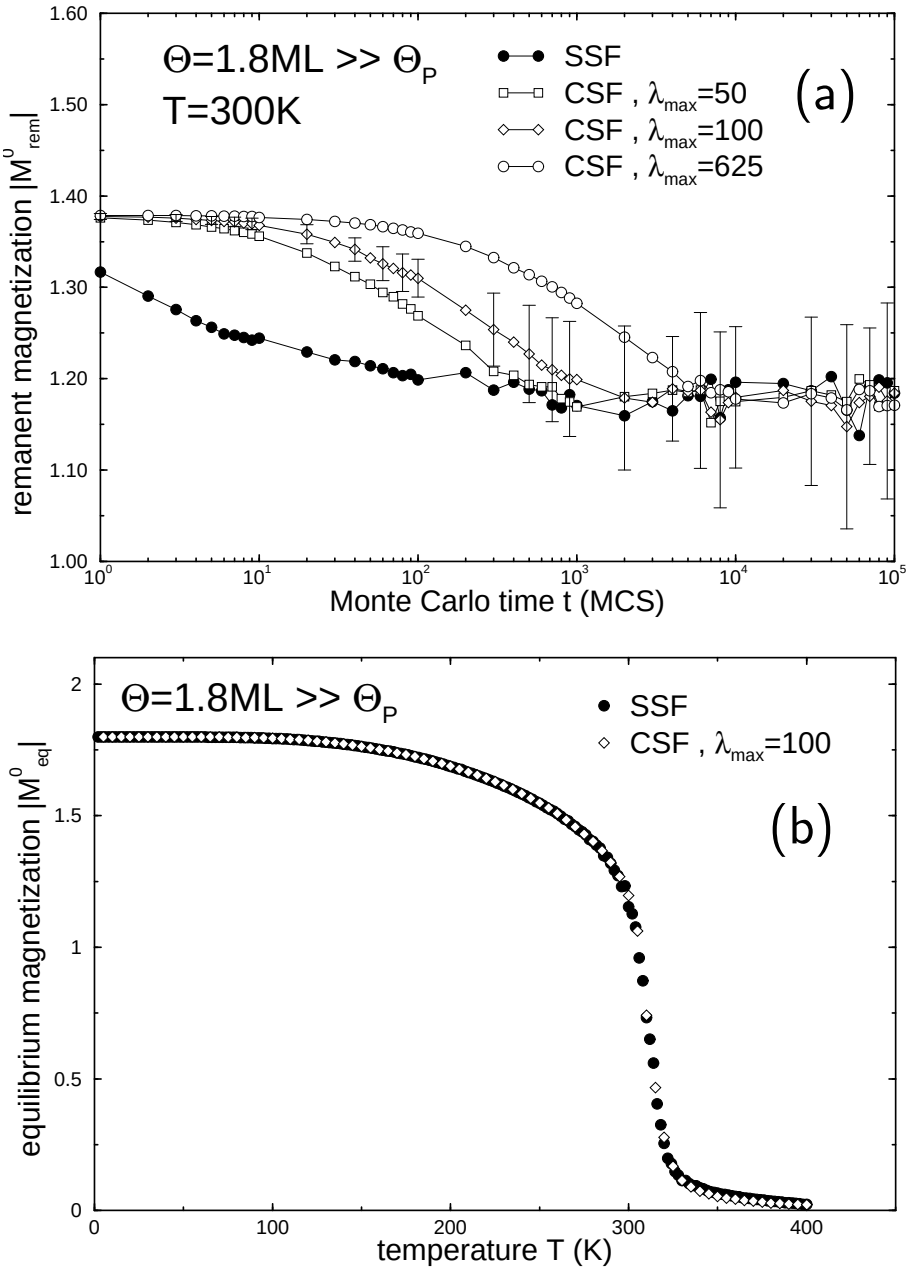

Figure 5.1: Comparison of the calculated film magnetization using the single-spin-flip (SSF) and the cluster-spin-flip (CSF) algorithm for a strongly connected film at coverage $\Theta = 1.8$ ML (monolayers), much larger than the percolation coverage $\Theta_{\mathrm{P}} = 0.9$ ML. (a) The remanent magnetization $|M^0_{\mathrm{rem}}(\Theta, T, t)|$ is plotted as function of MC time (MC steps) t for temperature $T = 300$ K. Only the inter-island exchange coupling is considered. Different maximum numbers $\lambda_{\max}$ of coherently flipping island spins within the CSF method are applied. All curves relax into the same stable value $|M^0_{\mathrm{rem}}(\Theta, T|$, as obtained by SSF. (b) The equilibrium magnetization $|M^0_{\mathrm{eq}}(\Theta, T)|$ is shown as function of temperature T. Excellent agreement between CSF and SSF is obtained. Here, $\lambda_{\max} = 100$ is applied.

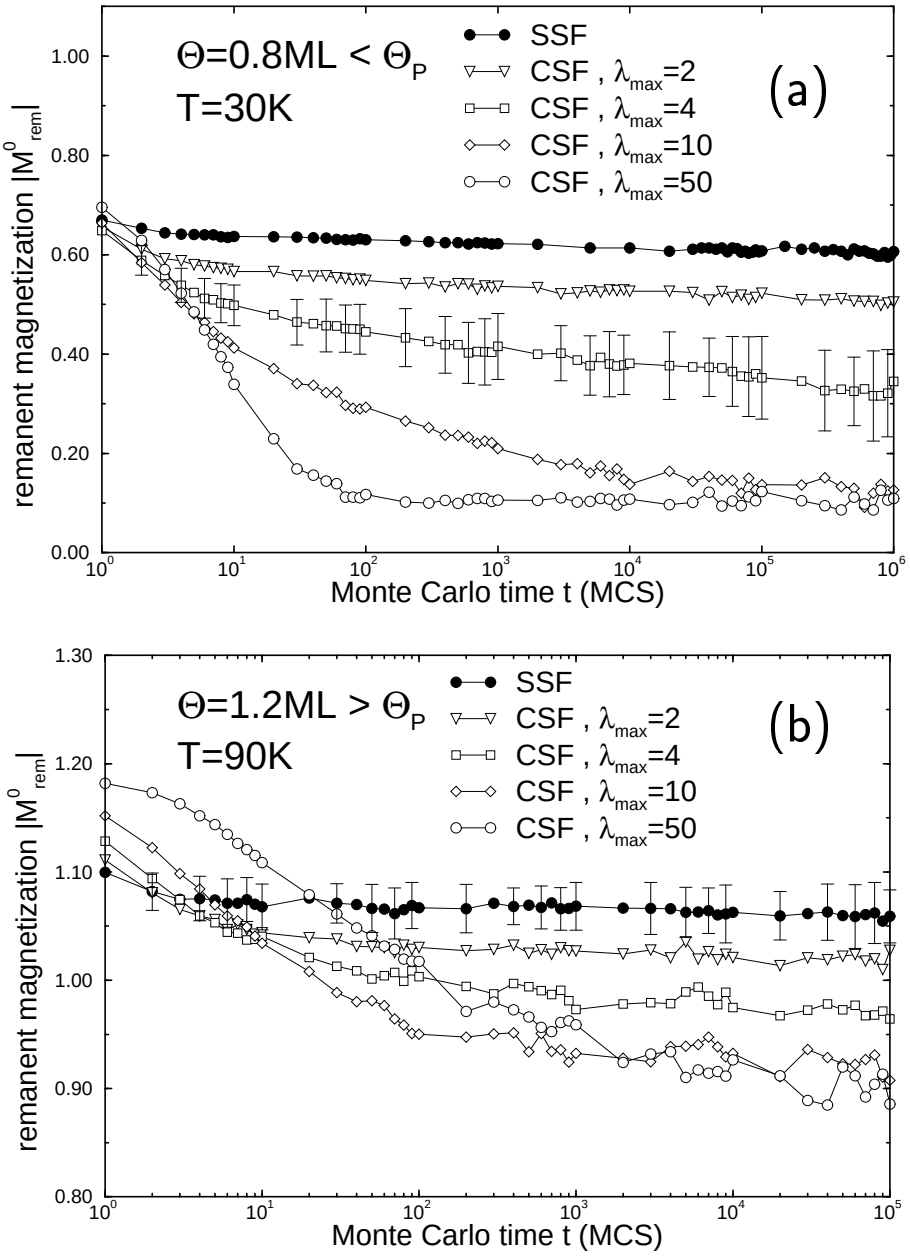

Figure 5.2: Comparison of the efficiency of the SSF and CSF algorithm for irregularly connected island structures below and above the percolation threshold $\Theta_{\mathrm{P}} = 0.9$ ML. The remanent magnetization $|M^0_{\mathrm{rem}}|$ as function of MC time (MC steps) t is shown. We use different maximum numbers $\lambda_{\max}$ of coherently flipping island magnetic moments within the CSF method. (a) $\Theta = 0.8$ ML $\lesssim \Theta_{\mathrm{P}}$: Only the CSF with $\lambda_{\max} \geq 10$ reaches the equilibrium value $|M^0_{\mathrm{eq}}| \approx 0.1$ within the depicted time range. (b) $\Theta = 1.2$ ML $\gtrsim \Theta_{\mathrm{P}}$: The CSF with $\lambda_{\max} = 10$ yields the fastest relaxation into the equlibrium value $|M^0_{\mathrm{eq}}| \approx 0.92$.

included. Due to the use of a finite unit cell and the absolute value, a finite but small $|M^0_{\mathrm{eq}}(\Theta, T)| \approx 0.1$ is obtained in our calculations, $|M^0_{\mathrm{eq}}| \propto Z_{\mathrm{eff}}^{-1/2}$, where Z_{eff} is the number of island clusters in the system. The SSF algorithm exhibits an extremely slow relaxation toward $|M^0_{\mathrm{eq}}|$. Even after 10^6 MCS (MC steps/spin) the remanent magnetization is relaxed only to $|M^0_{\mathrm{rem}}| = 0.60$, thus giving the wrong impression of a long-range ferromagnetic order. The reason for this behavior is that SSF considers very unfavorable spin states for relaxation, as discussed in Sec. 4.2.2. Already the allowance of a few coherently flipping island spins results in a much faster relaxation. The relaxation behavior converges rapidly with increasing $\lambda_{\max}$. Using CSF with $\lambda_{\max} = 50$ or larger, equilibrium is reached already after ~ 100 MCS. Clearly, to obtain a fast equilibration, $\lambda_{\max}$ must be chosen the larger, the closer the coverage to Θ_{P}, since the size of the island clusters increases.

The CSF algorithm leads to a much faster equilibration also for films with a percolating structure for coverages $\Theta \gtrsim \Theta_{\mathrm{P}}$, as demonstrated in Fig. 5.2 (b) for $\Theta = 1.2$ ML and temperature $T = 90$ K. In this coverage range, island clusters are present which have only *weak links* to other clusters, see Fig. 2.6 (f), p. 30. The percolating film structure leads to a ferromagnetic long-range order, indicated by a finite $|M^0_{\mathrm{eq}}| \approx 0.92$. Again, the SSF algorithm equilibrates the system very inefficiently, resulting in an overestimation of the long-range magnetic order. The fastest relaxation is obtained with $\lambda_{\max} = 10$, whereas the larger value $\lambda_{\max} = 50$ leads to a somewhat slower equilibration due to the same reasons as mentioned in connection with Fig. 5.1 (a).

To conclude, we have demonstrated that for irregularly connected island systems with and without a percolating island cluster, the application of the SSF algorithm leads to a strong overestimation of the long-range ferromagnetic order, which is avoided by applying CSF. Firstly, this results in an *efficient* equilibration of such systems into the 'true' thermodynamic equilibrium within accessible simulation times, which is a prerequisite for the investigation of partly coagulated systems for coverages $\Theta < \Theta_{\mathrm{P}}$, using the *equilibrium* MC method. Here, the inter-island dipole coupling, which is much weaker than the exchange coupling, could possibly lead to a long-range magnetic order. Secondly, we claim that CSF in comparison to SSF leads to a much more *realistic* magnetic relaxation in *kinetic* MC simulations, since coherent island magnetization rotations also occur in real systems, if the islands are strongly exchange coupled and the corresponding anisotropy barrier is sufficiently low. Thus, the application of CSF allows for a proper study of the magnetic ordering and relaxation of irregularly connected island systems, in particular, taking into account dipole interaction and anisotropy barriers. In the following calculations, we apply the CSF algorithm and set the maximum island cluster size $\lambda_{\max}$ equal to the total number of island

spins Z, except for coverages $\Theta \gg \Theta_{\mathrm{P}}$, where we yield a better efficiency and a more realistic relaxation for $\lambda_{\max} = 100$. We use the SSF algorithm exclusively for the study of noninteracting island systems and for systems, where the island spins are merely coupled by dipole interactions.

5.3 Long-range magnetic order

In this section, we present results for the effect of inter-island dipole and exchange couplings on the long-range magnetic order using the equilibrium MC method. The bilayer island growth mode (version I) is taken into account; film coverages Θ below and above the percolation threshold $\Theta_{\mathrm{P}} = 0.9$ ML are addressed. If not otherwise stated, the magnetic parameter set I of Tab. 5.1, p. 63, is used. The MC results are compared to results, obtained by the simple mean-field theory for long-range order, given in Appendix F.2.

As discussed in the Introduction of this thesis, for coverages $\Theta < \Theta_{\mathrm{P}}$ the long-range magnetic dipole coupling between islands and island clusters could lead to a long-range magnetic ordering. For this anisotropic coupling, in-plane island spins $S_i^x = \pm 1$, directed along the x axis, are assumed. For coverages $\Theta > \Theta_{\mathrm{P}}$, the inter-island exchange coupling (domain wall energy) γ_{ij} between coagulated islands is expected to result in a long-range ferromagnetic order with high Curie temperature T_{C}.

In the following, equilibrium properties are determined, which, within our two-state model $S_i = \pm 1$, are not affected by the single-island anisotropy K. Thus, exclusively Metropolis-type flip rates are used, given by Eq. (3.39), for which the magnetic relaxation is not slowed down by anisotropy barriers. If not otherwise stated, the CSF algorithm is applied. The MC process always starts from the fully aligned spin state.

5.3.1 Coverages below the percolation threshold

In this subsection, we present results on the combined effect of the inter-island dipole and exchange coupling on the film magnetization for coverages Θ below the percolation threshold $\Theta_{\mathrm{P}} = 0.9$ ML.

Fig. 5.3 shows the remanent magnetization $|M_{\mathrm{rem}}(\Theta, T, t)|$ for different temperatures T as a function of MC time (MC steps) t. The coverage is assumed to be $\Theta = 0.8\,\mathrm{ML} \lesssim \Theta_{\mathrm{P}}$. Starting from the saturated state $|M_{\mathrm{rem}}(\Theta, T, t = 0)| = 0.8$, the remanent magnetizations equilibrate during the first several hundred MC steps into *stable* values $|M_{\mathrm{rem}}| > |M_{\mathrm{rem}}^0|$, where for $|M_{\mathrm{rem}}^0|$ the dipole interaction is neglected. This indicates a long-range magnetic order $|M_{\mathrm{eq}}(\Theta, T)|$ due to the inter-island dipole coupling.

In Fig. 5.4, the equilibrium magnetization $|M_{\mathrm{eq}}(\Theta, T)|$ is shown as function of temperature T for different coverages $\Theta < \Theta_{\mathrm{P}}$. For low temperatures,

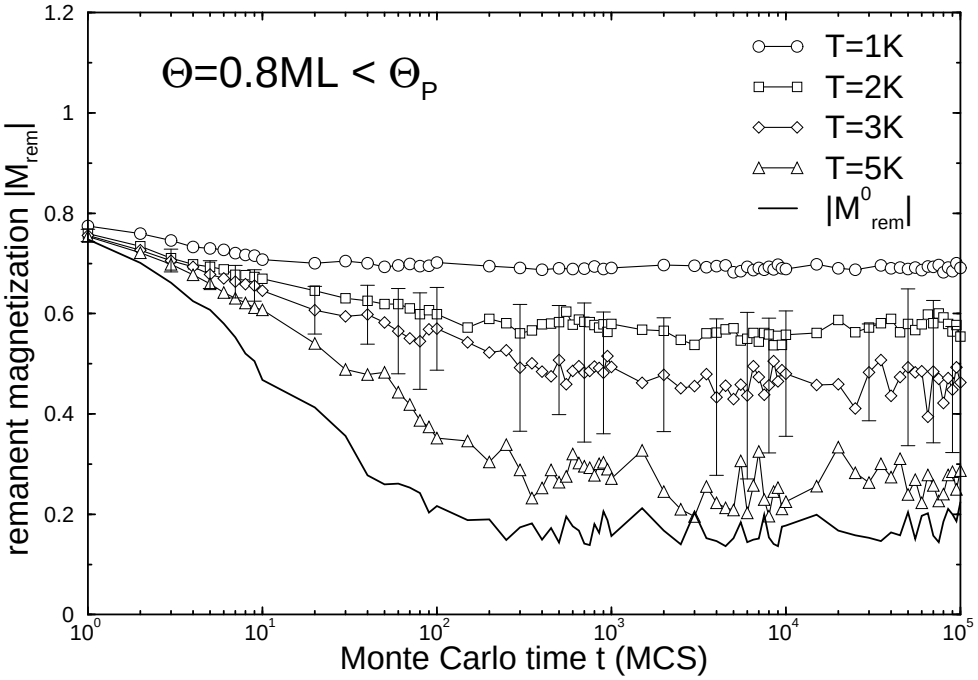

Figure 5.3: Long-range magnetic ordering due to dipole interaction. The remanent magnetization $|M_{\rm rem}(\Theta, T, t)|$ is plotted as function of MC time (MC steps) t for coverage $\Theta = 0.8$ ML $< \Theta_{\rm P}$ and different temperatures T. For $|M^0_{\rm rem}|$ the dipole interaction is neglected. Stable, dipole-coupling induced magnetizations $|M_{\rm rem}| > |M^0_{\rm rem}|$ are obtained for low temperatures.

clearly a magnetic order due to the dipole interaction is seen, which becomes larger for increasing Θ, since then the average island cluster size, and thus the average dipole coupling energy of the clusters, increases. Above the ordering temperatures $T_{\rm C}(\Theta)$, the magnetizations $|M_{\rm eq}(\Theta, T)|$ reach the corresponding values $|M^0_{\rm eq}(\Theta, T)|$ as calculated without the dipole interaction. Remember that due to the utilization of absolute values, $|M^0_{\rm eq}|$ does not vanish, rather a small value $|M^0_{\rm eq}| \propto Z_{\rm eff}^{-1/2}$ results, where $Z_{\rm eff}$ is the number of island clusters in the system. In the following, $T_{\rm C}(\Theta)$ is estimated by extrapolating the linear part of $|M_{\rm eq}|$ to $|M^0_{\rm eq}|$. The ordering temperature, even for the largest investigated coverage shortly below the percolation threshold $\Theta_{\rm P}$, is quite low, yielding $T_{\rm C} \approx 6$ K for $\Theta = 0.8$ ML. The rounding of $|M_{\rm eq}|$ near the ordering temperature is caused by (i) the finite size of the unit cell, (ii) the use of the absolute value, (iii) the presence of an island-size and -position dispersion, and (iv) the average over different realizations of the unit cell.

Next, we investigate the role of the inter-island exchange coupling γ in film structures without percolation. In Fig. 5.5 (a), we present results for systems where the islands are solely coupled by the dipole interaction. Here,

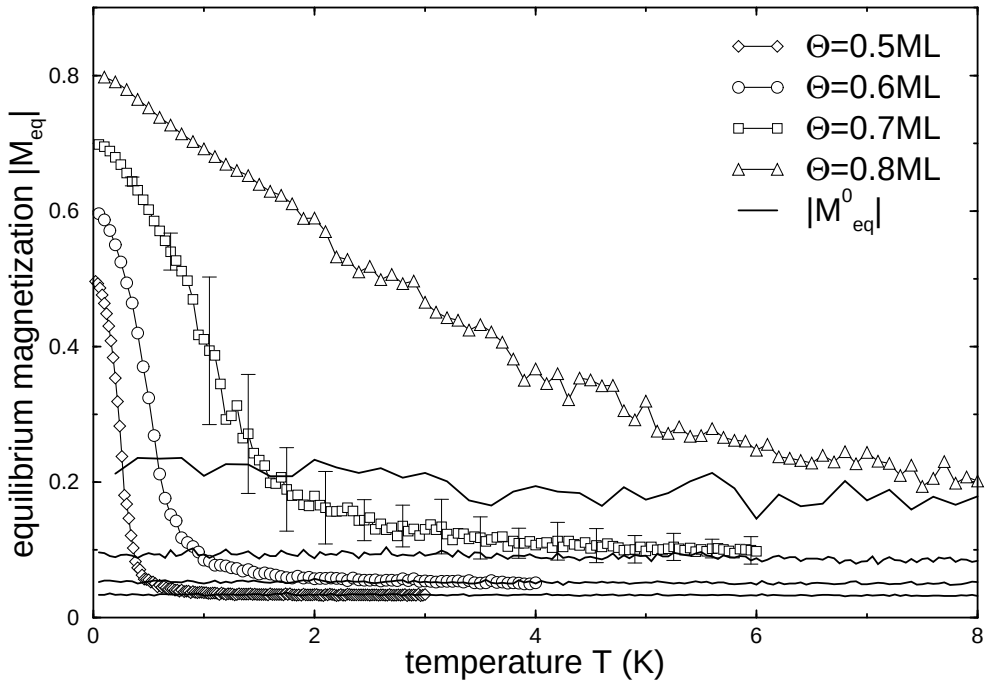

Figure 5.4: Long-range magnetic ordering due to dipole interaction. The equilibrium magnetization $|M_{\mathrm{eq}}(\Theta, T)|$ is depicted as function of temperature T for different coverages $\Theta < \Theta_{\mathrm{P}} = 0.9$ ML. The quantities $|M^0_{\mathrm{eq}}(\Theta, T)|$ neglect the dipole interaction.

the exchange coupling between neighboring islands is neglected ($\gamma = 0$). The equilibrium magnetization $|M_{\mathrm{eq}}(\Theta, T)|$ is shown as function of temperature T for different coverages Θ up to 2 ML. In such systems, the dipole coupling results in very low ordering temperatures T_{C}.

A comparison of these results for coverages $\Theta < \Theta_{\mathrm{P}}$ to results shown above, where the exchange coupling is included ($\gamma = 5.6$ meV), is presented in Fig. 5.5 (b). For $\Theta = 0.5$ ML, similar magnetization curves are obtained in both cases, since for this coverage only few islands are exchange-coupled to each other. However, for the larger coverage $\Theta = 0.8$ ML, the short-range exchange coupling leads to a much higher ordering temperature T_{C}. This is due to the fact that at low temperatures the exchange interaction aligns connected islands, thus leading to larger effective magnetic moments and dipole energies E_{dip}. In the depicted temperature range, an infinite inter-island exchange coupling $\gamma = \infty$ yields practically the same results for both coverages 0.5 and 0.8 ML (not shown). We conclude that the long-range dipole coupling between islands leads to the *existence* of a long-range magnetic order for systems without a percolating island cluster. The *height* of the ordering temperature is strongly influenced by the connectivity of the

irregular island system and the inter-island exchange interaction.

Finally, in Fig. 5.6, the obtained ordering temperatures $T_C(\Theta)$ are depicted for different film coverages Θ below the percolation threshold $\Theta_P = 0.9$ ML of the bilayer island growth mode. The lines connecting the symbols are drawn as guides to the eye. Approaching Θ_P, a strong increase of T_C can be seen, if the exchange interaction $\gamma = 5.6$ meV between islands is included. Evidently, by neglect of the exchange coupling ($\gamma = 0$), a distinct variation of $T_C(\Theta)$ near Θ_P is not obtained.

The existence of a long-range magnetic ordering of a 2D spin system due to dipole interaction has been calculated by De'Bell *et al.* for a periodic *uniform* square lattice with XY-vector spins using a MC method and interacting spin-wave theory [37, 38]. We find for the first time that also within *irregular* island systems below the percolation threshold the dipole interaction leads to a magnetic ordering below a nonzero critical temperature. Thermal fluctuations are explicitly taken into account by the MC method. Since we applied in-plane, two-state island spins $S_i^x = \pm 1$, the long-range ordering is indicated by a net magnetization $|M_{eq}| > |M_{eq}^0|$. We expect such a collective state due to dipole interaction to be spin-glass-like [11], as recently proposed by several authors for 3D systems of separated magnetic particles [5, 40, 81]. This interesting problem needs further investigation. We remark that the obtained ordering temperatures T_C will increase by consideration of noncollinear island spin configurations beyond $S_i = \pm 1$ [80], which lower the average dipole energy, and by taking into account the finite island extension for the dipole interaction beyond the point dipole approximation [79]. However, the order of magnitude of T_C is expected to be the same as calculated in the present study. Assuming 3D islands, covering the same substrate surface area as the *flat* bilayer islands, *much* larger ordering temperatures will result due to the strongly increased island magnetic moments.

5.3.2 Coverages above the percolation threshold

In this subsection, we investigate the equilibrium film magnetization for coverages Θ above the percolation threshold $\Theta_P = 0.9$ ML of the bilayer growth mode. Inter-island exchange and dipole interactions are taken into account.

In Fig. 5.7, the equilibrium magnetization $|M_{eq}(\Theta, T)|$ is shown as function of temperature T for different coverages $\Theta > \Theta_P$. The strong exchange coupling causes a long-range ferromagnetic order up to high temperatures. For large Θ, the behavior of $|M_{eq}|$ at low T is reigned by the decrease of the *internal* island magnetization $m_i(\Theta, T)$, as obtained by the mean-field approach, Eqs. (F.1) and (F.2), given in Appendix F.1. At elevated temperatures, a strong decay of $|M_{eq}|$ is caused by the disturbance of the island spin alignment due to thermal fluctuations. With decreasing coverage, the ordering temperature T_C is shifted to lower temperatures, since the average

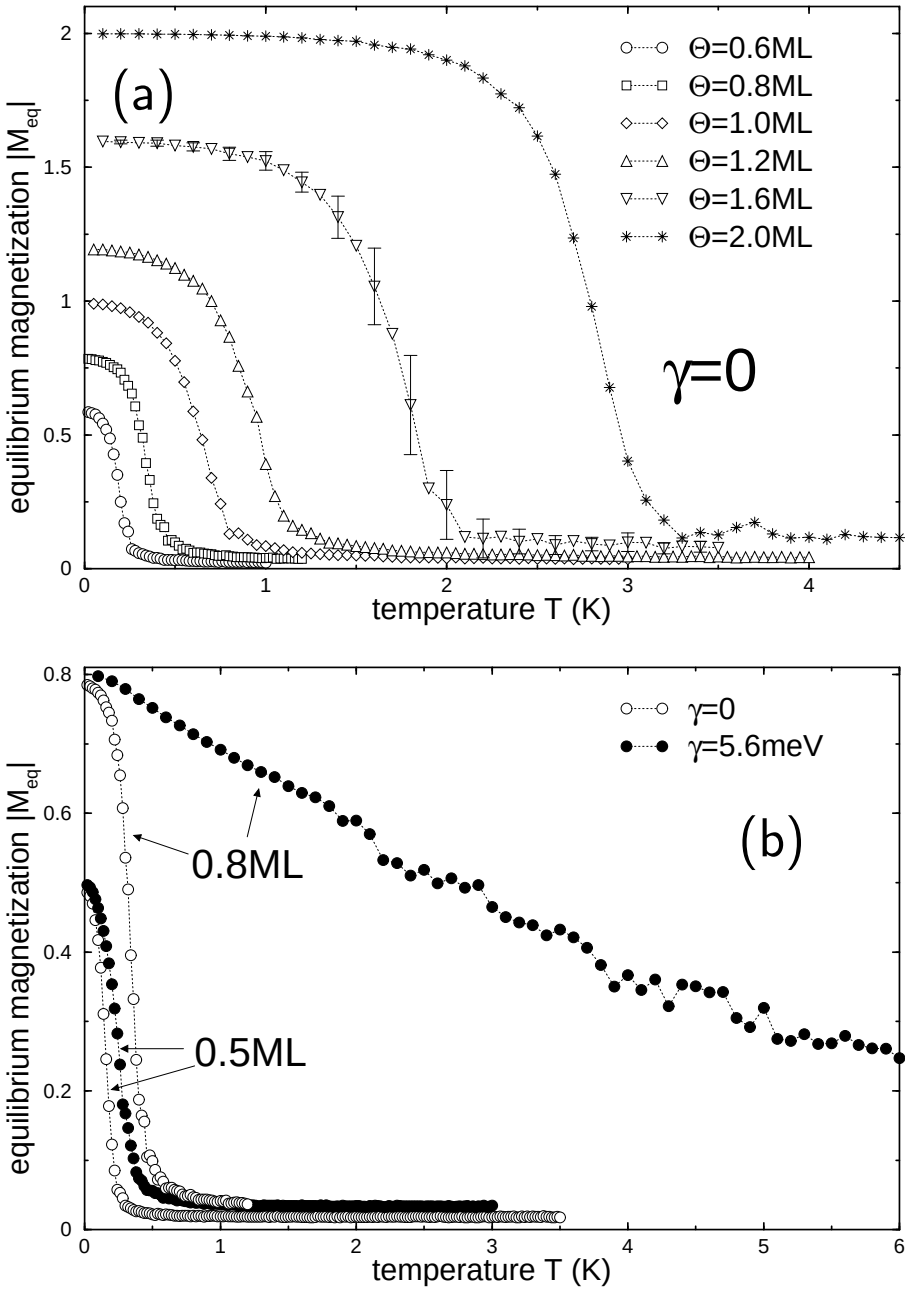

Figure 5.5: Equilibrium magnetization $|M_{\rm eq}(\Theta, T)|$ as function of temperature T for different coverages Θ, taking into account the inter-island dipole interaction. (a) The inter-island exchange coupling γ is neglected. (b) Comparison for two different coverages $\Theta < \Theta_{\rm P} = 0.9$ ML: for the filled circles (•), the inter-island exchange coupling $\gamma = 5.6$ meV is included, whereas for the open circles (○) this interaction is neglected.

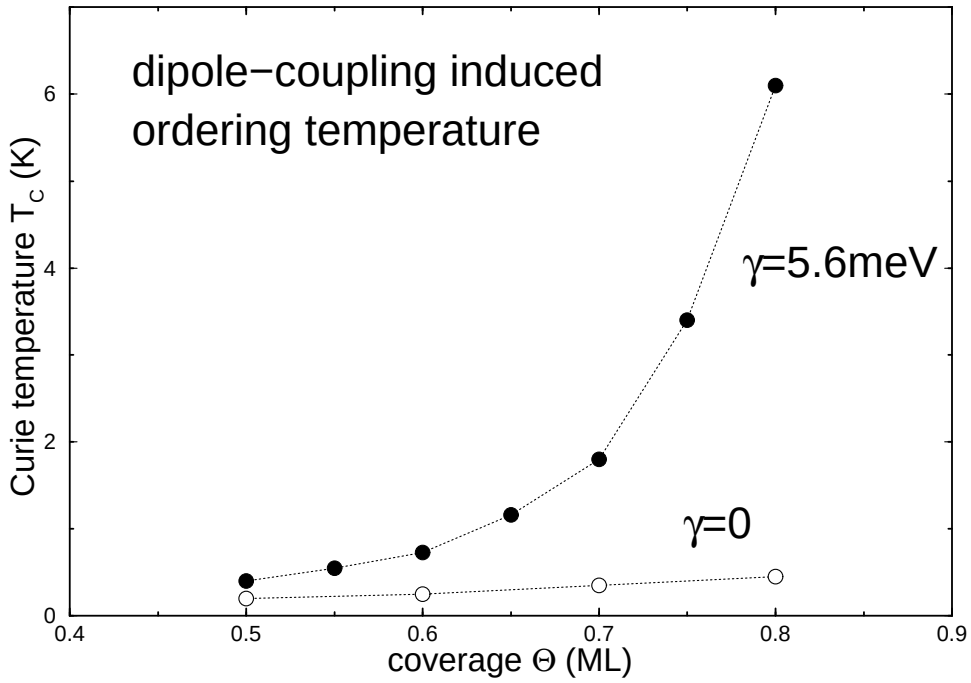

Figure 5.6: The ordering temperature $T_{\mathrm{C}}(\Theta)$ of the long-range magnetic order is plotted for different coverages Θ below the percolation threshold $\Theta_{\mathrm{P}} = 0.9$ ML. The filled circles (•) include the exchange coupling γ between islands, the open circles (∘) neglect this interaction.

exchange energy between islands decreases due to the diminished connectivity of the system. Here, the transition from ferromagnetically ordered to disordered (superparamagnetic) high-temperature states becomes less pronounced.

A very small effect of the dipole interaction on the magnetization is visible only at very low temperatures and for coverages close to the percolation threshold, $\Theta \gtrsim \Theta_{\mathrm{P}}$. To present an example, in Fig. 5.7, the filled symbols neglect the dipole interaction for $\Theta = 1.0$ ML. The inclusion of the dipole interaction leads to a small peak of $|M_{\mathrm{eq}}|$ at very low temperatures, which is indicated by the arrow. This small peak results from few isolated islands or island clusters, which are coupled by the long-range dipole interaction to the ferromagnetically ordered, percolating cluster, see Fig. 2.6 (e), p. 30.

In Fig. 5.8, the resulting high ordering temperatures $T_{\mathrm{C}}(\Theta)$ are plotted for different coverages $\Theta > \Theta_{\mathrm{P}}$. The ordering temperatures are deduced from Fig. 5.7, by extrapolating the linear parts of $|M_{\mathrm{eq}}(\Theta, T)|$. The line connecting the symbols is drawn to guide the eye. We observe that the slope of the line becomes smaller for increasing coverage.

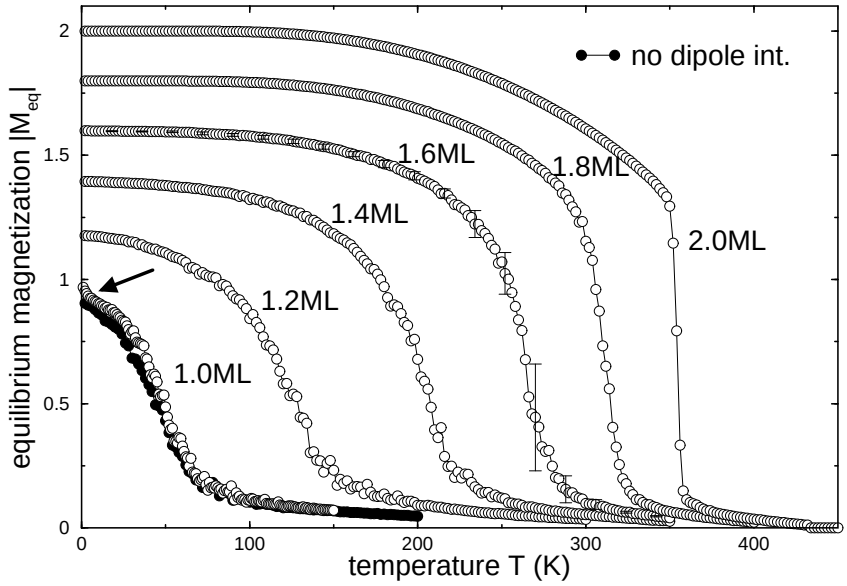

Figure 5.7: Long-range ferromagnetic ordering for different film coverages Θ above the percolation coverage $\Theta_{\mathrm{P}} = 0.9$ ML. The equilibrium magnetization $|M_{\mathrm{eq}}(\Theta, T)|$ is shown as function of temperature T. Inter-island exchange and dipole couplings are taken into account. For $\Theta = 1.0$ ML, the small ordering effect due to dipole interaction is indicated by an arrow.

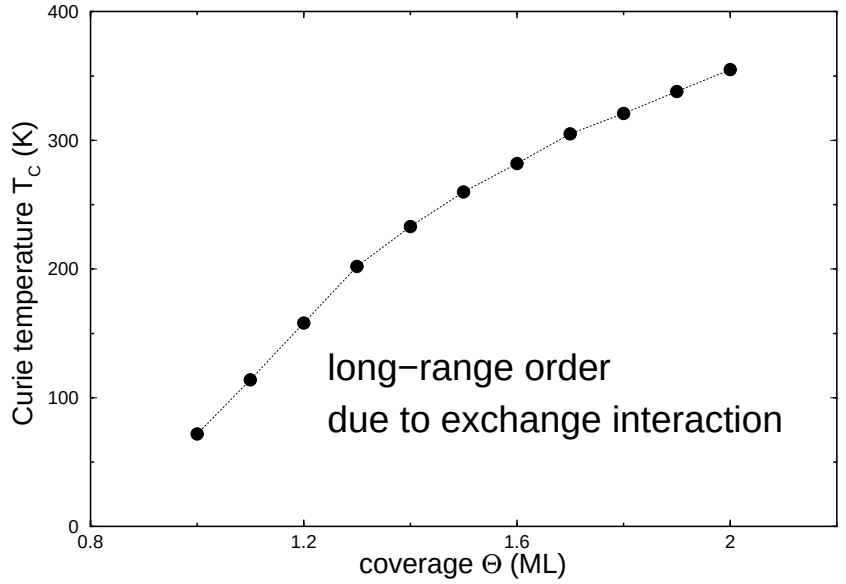

Figure 5.8: The Curie temperature $T_{\mathrm{C}}(\Theta)$ is plotted for different coverages $\Theta > \Theta_{\mathrm{P}} = 0.9$ ML.

5.3.3 Comparison with MFT results

For a comparison to cluster MC results, we recalculated the long-range magnetic order for the entire coverage range, investigated in the two previous subsections, using a simple mean-field theory (MFT), introduced in Appendix F.2. Exchange and dipole interactions between island spins $S_i^x = \pm 1$ are taken into account. We applied identical structural and magnetic parameters as used in the MC simulations, except for the inter-island exchange interaction γ, which will be explained below. Again, the magnetizations are obtained by averaging over at least 20 different structural realizations of the unit cell.

Fig. 5.9 shows results for the equilibrium magnetization $M_{\mathrm{MFT}}(\Theta, T)$ as function of temperature T for different film coverages Θ. In Fig. 5.9 (a), only the dipole interaction between the island spins is taken into account; the inter-island exchange interaction is neglected ($\gamma = 0$). The shapes of the curves are similar to the ones obtained by the MC method, shown in Fig. 5.5 (a), p. 73. However, the corresponding ordering temperatures, above which the M_{MFT} vanish, are by a factor ~ 30 larger than calculated in the MC simulations. This demonstrates the importance of thermal fluctuations in 2D systems of dipole-coupled magnetic particles, which are neglected in the mean-field approach.

For the results presented in Fig. 5.9 (b), in addition to the dipole coupling the exchange interaction γ between magnetic islands is taken into account. For a better comparison with MC results, γ is adjusted to give the *same* Curie temperature $T_{\mathrm{C}} = 355$ K of the long-range ferromagnetic order at coverage $\Theta = 2$ ML. This results in $\gamma = 0.28$ meV, which is by a factor 20 smaller than the value used in the MC calculations, since MFT neglects thermal fluctuations and the low dimension of the system. To investigate the effect of the dipole coupling, this interaction is neglected for the calculations of the dotted lines. For coverages Θ, much larger than the percolation threshold $\Theta_{\mathrm{P}} = 0.9$ ML, the MFT results are in rough agreement with the MC data of Fig. 5.7, p. 75. We observe that for the depicted coverages the dipole coupling plays only a minor role for the long-range order, obtained by MFT. However, this also holds for systems *without* a percolating island cluster at coverages $\Theta = 0.5$ and 0.7 ML. Here, MFT predicts a long-range magnetic order neglecting the long-range coupling, which is obviously wrong. This behavior results from the fact, that the simple MFT predicts a finite film magnetization as long as a single finite spin expectation value $\langle S_i \rangle$, described by Eq. (F.12), is present. This results already from a pair of exchange-coupled islands, see Fig. 2.6 (b), (c), p. 30.

For a comparison, the resulting ordering temperatures $T_{\mathrm{C}}(\Theta)$ obtained by the cluster MC method and the simple MFT are summarized in Fig. 5.10 for the entire investigated coverage range. We conclude that MFT produces

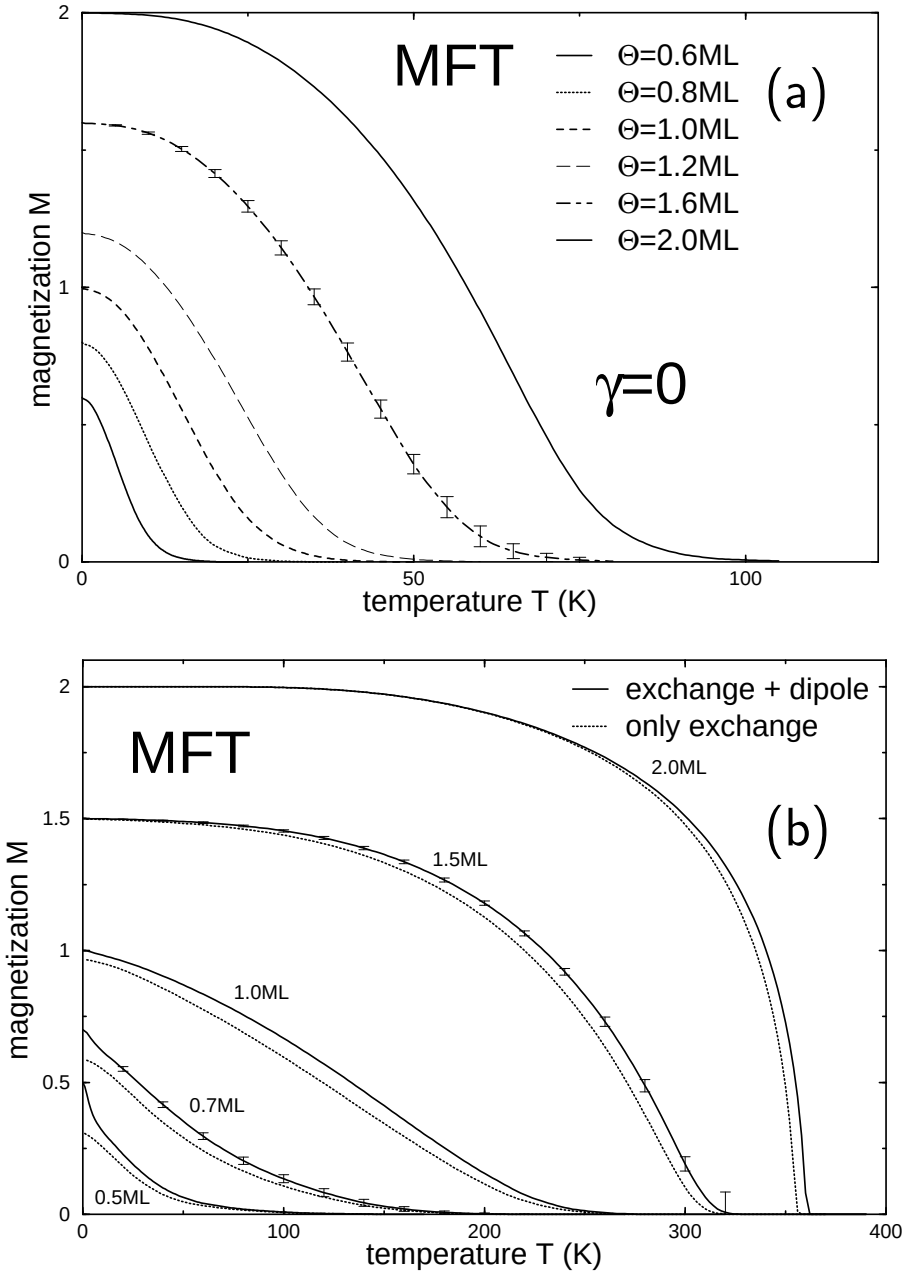

Figure 5.9: The film magnetization $M_{\mathrm{MFT}}(\Theta, T)$ obtained by the mean-field theory (MFT), see Appendix F.2, is shown as function of temperature T. Curves for different film coverages Θ are depicted. (a) Exclusively the inter-island dipole coupling is taken into account; the exchange coupling γ is neglected. (b) In addition to the dipole coupling a finite exchange coupling $\gamma = 0.28$ meV between connected islands is included, resulting in $T_{\mathrm{C}}^{\mathrm{MFT}}(2\,\mathrm{ML}) \approx 355$ K. For a comparison, the dotted lines neglect the dipole coupling.

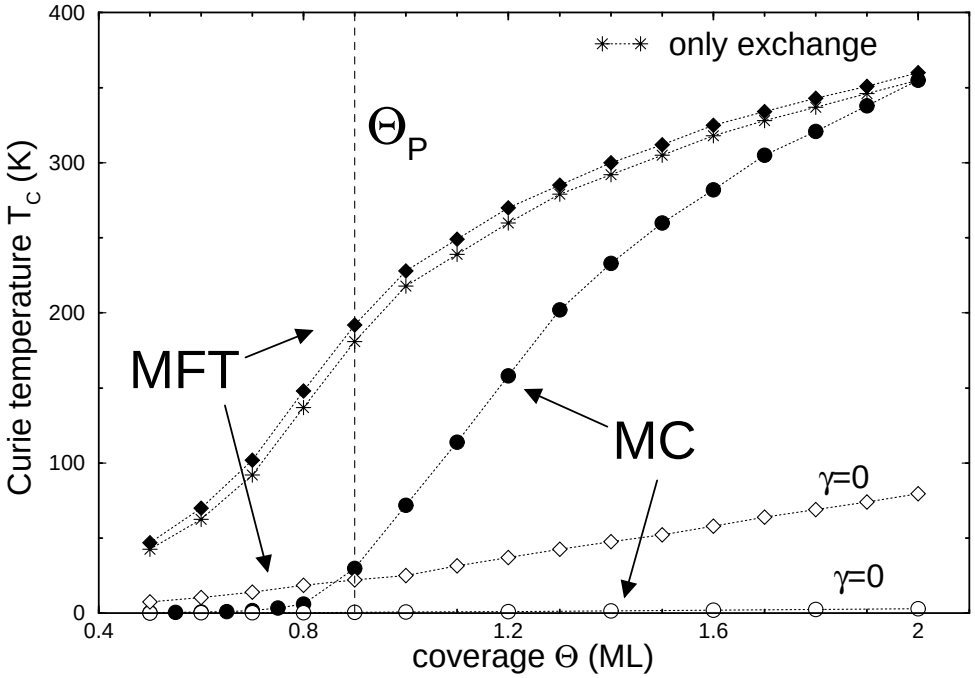

Figure 5.10: Comparison of the simple MFT and the cluster MC method. The resulting Curie temperatures $T_C(\Theta)$ are plotted for the entire investigated coverage range. The circles refer to MC results, the diamonds and stars to MFT results. For the filled symbols both exchange and dipole couplings are taken into account, for the open symbols the inter-island exchange coupling γ is neglected. The stars were calculated by neglect of the dipole coupling. The dashed line indicates the percolation threshold $\Theta_P = 0.9$ ML.

qualitatively reasonable results for strongly connected films at film coverages $\Theta \gg \Theta_P$ and for coverages $\Theta \ll \Theta_P$, where the islands are exclusively dipole-coupled. However, due to the neglect of the low dimensionality of the system and thermal fluctuations, the ordering temperatures are *strongly* overestimated by MFT. For intermediate coverages, where the magnetic islands are irregularly connected, the simple MFT is not suited, since it overestimates the long-range magnetic order due to inter-island exchange coupling. In particular, the prediction of a long-range order for systems without a percolating island cluster is an artefact of the method.

5.4 Magnetic relaxation

This section presents results on the magnetic relaxation behavior from the aligned island spin state towards thermodynamical equilibrium using the kinetic MC method. The influence of energy barriers ΔE resulting from the

single-island magnetic anisotropy K, and of inter-island dipole and exchange couplings is investigated. The bilayer island growth mode (version I) is taken into account. Film coverages Θ below and above the percolation threshold $\Theta_{\mathrm{P}} = 0.9$ ML are studied. If not otherwise stated, the magnetic parameter set I of Tab. 5.1, p. 63, is used.

As discussed in Sec. 3.2.2, single-island anisotropy energy barriers have a strong effect on the magnetic relaxation of *noninteracting* island systems. At low temperatures a finite nonequilibrium remanent magnetization can be observed for long waiting times. Here, we turn to results on the combined action of anisotropy barriers and inter-island interactions on the magnetic relaxation of irregular island systems. For strongly connected films, we expect only a weak influence of anisotropy barriers due to the strong exchange fields. For the effect of the anisotropic dipole coupling on the relaxation, both in-plane and out-of-plane island spin systems are studied.

For the kinetic MC simulations, the Néel-Brown model and Metropolis-type flip rates (Eqs. (3.37) and (3.39)) are used, depending on the value of the local effective field (Eq. (3.41)). Here, $\Delta t = 1$ MCS (MC step/spin) refers to the physical time step $\Delta t' = 0.1$ sec. Within the two-state spin model $S_i = \pm 1$, a finite single-island magnetic anisotropy K does not influence the equilibrium magnetization $|M_{\mathrm{eq}}|$. Thus, in this section we study the magnetic relaxation into states which were investigated in the previous section.

5.4.1 Coverages below the percolation threshold

In this subsection, we show results on the influence of the single-island anisotropy K and the inter-island exchange interaction (domain wall energy) γ_{ij} on the magnetic relaxation for film coverages Θ below the percolation threshold $\Theta_{\mathrm{P}} = 0.9$ ML. The inter-island dipole coupling is neglected.

In Fig. 5.11, the remanent film magnetization $|M_{\mathrm{rem}}(\Theta, T, t)|$ is given as function of MC time t for different temperatures T. The coverage is assumed to be $\Theta = 0.8$ ML, slightly below Θ_{P}. An anisotropy parameter $K = 0.01$ meV is applied. Starting from the fully aligned island spin state $|M_{\mathrm{rem}}(t = 0)| \approx 0.8$, first, $|M_{\mathrm{rem}}|$ drops rapidly due to thermally activated rotations of single-island spins and small island-spin clusters. The further relaxation happens much more slowly, since here larger spin clusters have to be reversed. For $T \gtrsim 25$ K the magnetization $|M_{\mathrm{rem}}|$ reaches within the depicted time range the curve $|M^0_{\mathrm{rem}}|$ as calculated for vanishing anisotropy $K = 0$. The dashed line indicates the time $t = 1000$ MCS (MC step/spin), which will be the time range of the subsequent simulations.

In Fig. 5.12, the symbols denote $|M_{\mathrm{rem}}(\Theta, T, t)|$ as function of temperature T for different coverages Θ. For all temperatures, $|M_{\mathrm{rem}}|$ is monitored after $t = 1000$ MCS, starting from the fully aligned state. Two different anisotropy parameters were applied, (a) $K = 0.01$ meV and (b) $K = 0.1$ meV. With in-

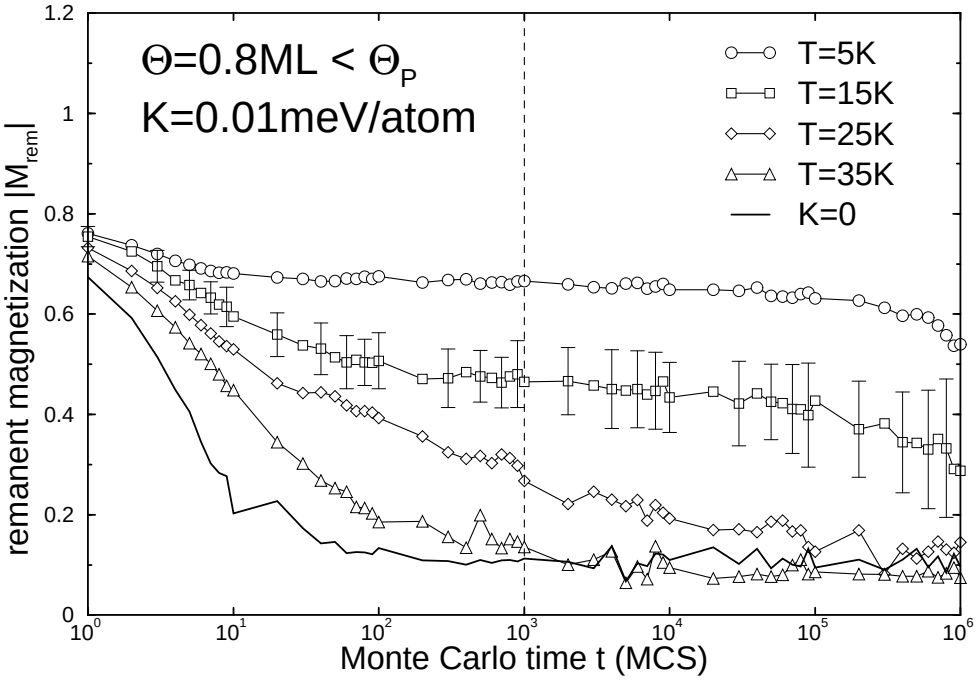

Figure 5.11: Relaxation of the remanent magnetization $|M_{\rm rem}(\Theta, T, t)|$ as function of MC time t for coverage $\Theta = 0.8$ ML $< \Theta_{\rm P} = 0.9$ ML and different temperatures T. The single-island anisotropy $K = 0.01$ meV and the inter-island exchange coupling are taken into account. For $T \geq 25$ K, the system relaxes into thermal equilibrium within the simulation time. The full line refers to $K = 0$ and $T = 35$ K. The dashed line denotes the time $t = 1000$ MCS (MC step/spin).

creasing temperature, the magnetization $|M_{\rm rem}(t = 10^3\,{\rm MCS}, T)|$ approaches the equilibrium value $|M^0_{\rm eq}| \approx 0$. The corresponding blocking temperatures $T_{\rm b}(\Theta, K, t)$ are estimated by extrapolating the linear parts of $|M_{\rm rem}(\Theta)|$ to $|M^0_{\rm eq}(\Theta)|$. A rounding of $|M_{\rm rem}|$ near $T_{\rm b}$ is observed due to the same reasons as discussed in the previous section in connection with Fig. 5.4. We observe that an increase of the single-island anisotropy K by a factor of 10 does not necessarily lead to an increase of $T_{\rm b}(\Theta, K)$ by the same factor; e. g. for $\Theta = 0.5$ ML the blocking temperature increases by a factor 5, and for $\Theta = 0.8$ ML by a factor 2. A proportionality $T_{\rm b} \propto K$ is predicted by the simple Stoner-Wohlfarth model for *coherent rotations* of connected island spins, which results in anisotropy barriers $\Delta E \propto K$, Eq. (3.17). The interesting deviating behavior is caused by *internal cluster excitations* due to the finite inter-island exchange coupling, i. e. by the creation or motion of domain walls inside clusters of coagulated islands.

In Fig. 5.13, the resulting blocking temperatures $T_{\rm b}(\Theta, K, t)$ are plotted in the coverage range $\Theta < \Theta_{\rm P} = 0.9$ ML for the assumed waiting time

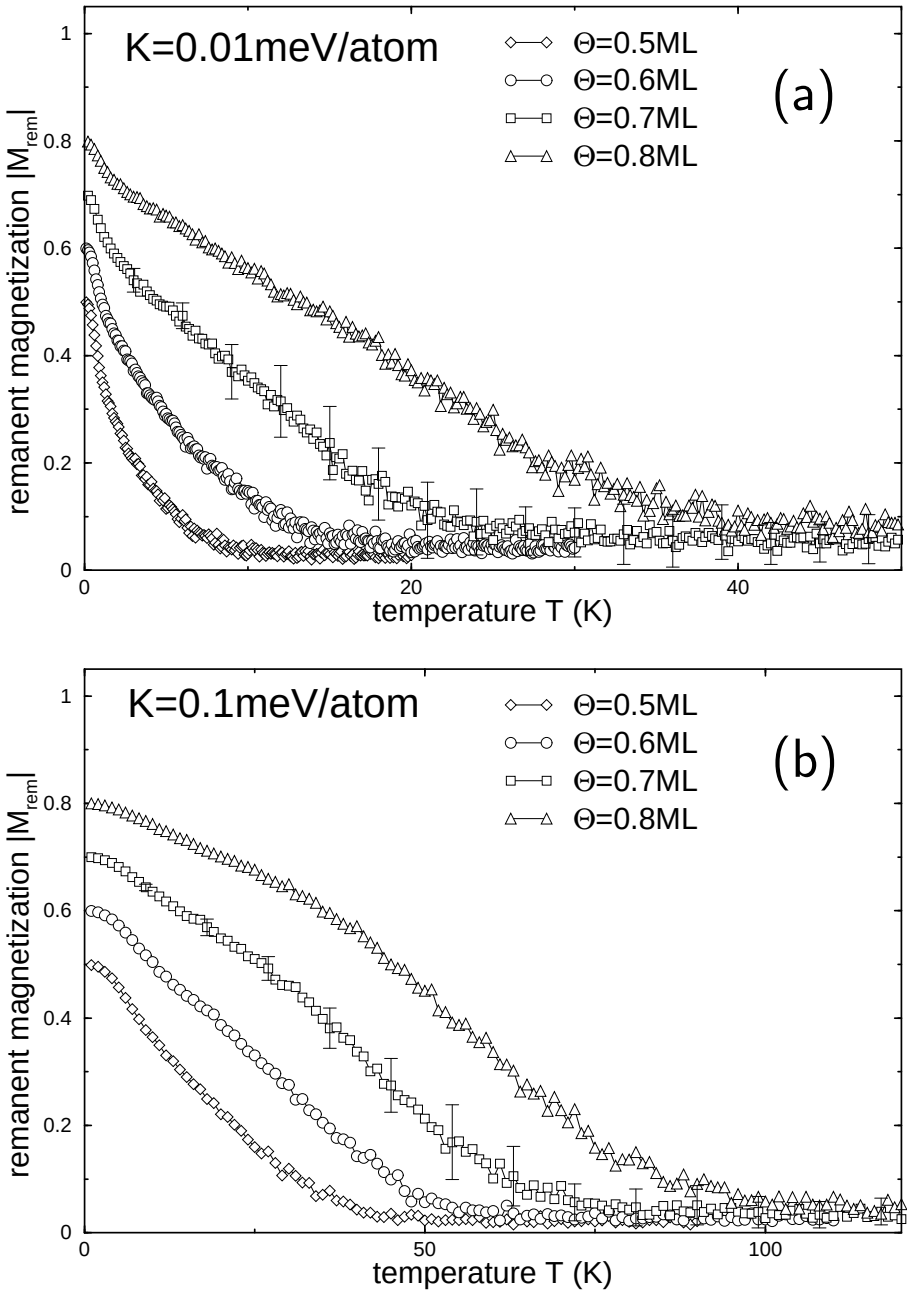

Figure 5.12: The remanent magnetization $|M_{\rm rem}(\Theta, T, t)|$ is shown as function of temperature T for two anisotropies, (a) $K = 0.01$ meV and (b) $K = 0.1$ meV. Only single-island anisotropy barriers and inter-island exchange couplings $\gamma = 5.6$ meV are taken into account. Different coverages $\Theta < \Theta_{\rm P} = 0.9$ ML are assumed. For all temperatures $|M_{\rm rem}|$ is calculated after $t = 1000$ MCS, starting from the fully aligned state.

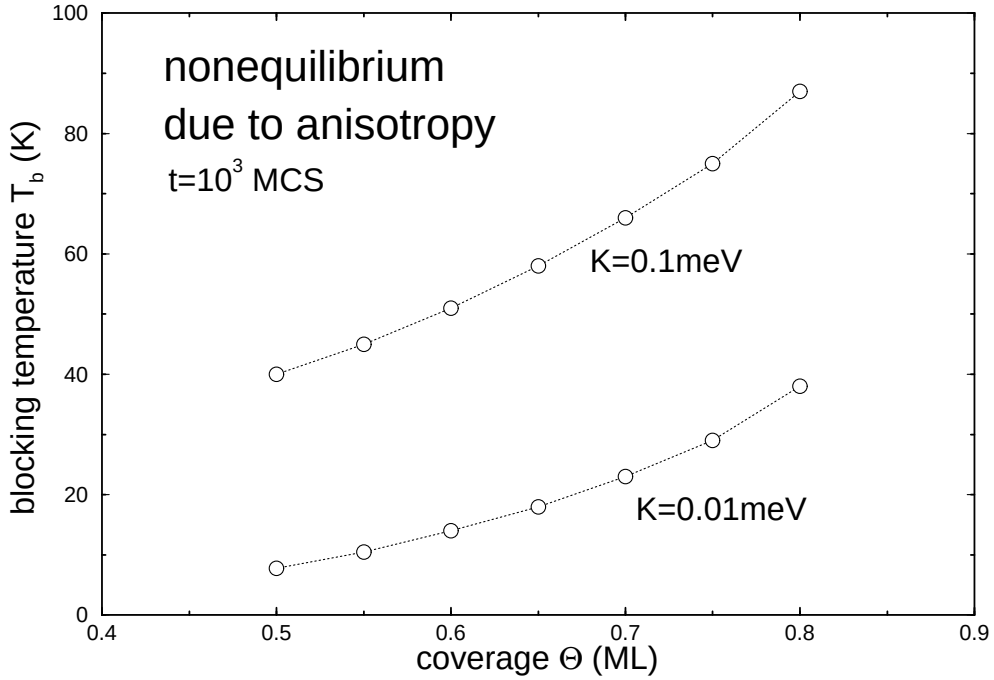

Figure 5.13: The blocking temperatures $T_\mathrm{b}(\Theta, K, t)$ are plotted for film coverages $\Theta < \Theta_\mathrm{P} = 0.9$ ML. A time $t = 1000$ MCS is assumed. Results for two different values of the single-island anisotropy K are depicted.

$t = 1000$ MCS. Two different anisotropy parameters $K = 0.01$ and 0.1 meV were investigated. Note again the lacking proportionality between T_b and K for increasing Θ.

To understand the role of a finite inter-island exchange coupling γ on the magnetic relaxation, we have performed additional calculations which are presented in Fig. 5.14. Again, the open symbols denote the remanent magnetization $|M_\mathrm{rem}|$ after $t = 1000$ MCS as function of temperature T for two different coverages, $\Theta = 0.6$ and 0.8 ML, as shown in Fig. 5.12 for the two anisotropy parameters. The dashed lines indicate results for $\gamma = 0$. The full lines are obtained for an infinite inter-island exchange coupling $\gamma = \infty$, hence allowing only for coherent rotations of connected island spins. For the uncoupled case, $|M_\mathrm{rem}|$ vanishes at low temperatures, since comparably small single-island energy barriers $\Delta E_i = N_i K_i$ have to be surmounted by thermal activation. A comparison between the dashed curves in (a) and (b) of Fig. 5.14 shows that the corresponding blocking temperatures T_b deviate by the factor 10, as expected. In the initial temperature range, the curves for finite inter-island exchange coupling $\gamma = 5.6$ meV follow the dashed lines. Thus, at these low temperatures, the relaxation evolves by rotations of separated single islands. Above a certain temperature (indicated in (b)

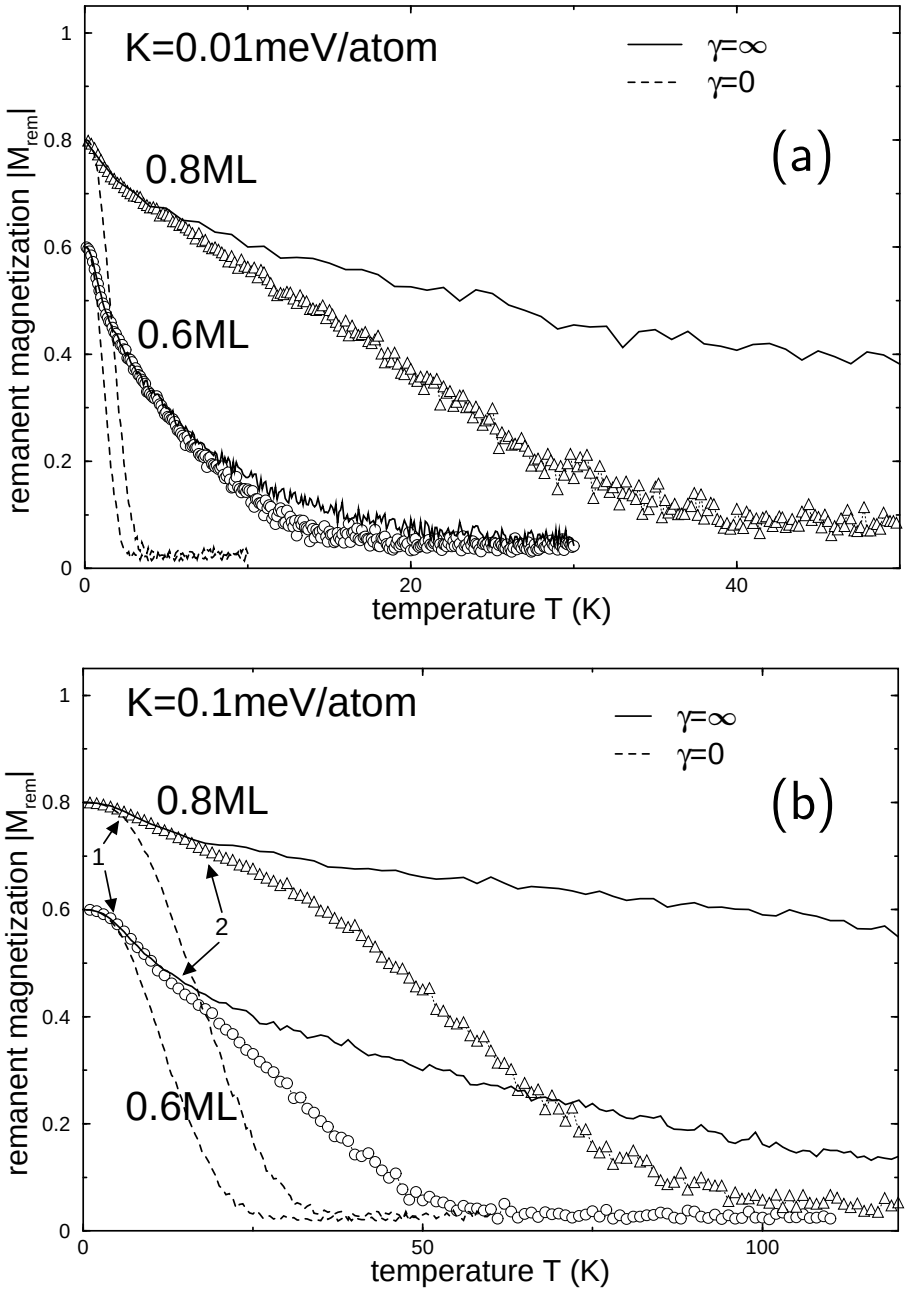

Figure 5.14: The remanent magnetization $|M_{\rm rem}(\Theta, T, t)|$ is shown as function of temperature T for two anisotropy constants, (a) $K = 0.01$ meV and (b) $K = 0.1$ meV. Two different coverages $\Theta < \Theta_{\rm P}$ are assumed. For comparison, the dashed lines refer to uncoupled spins using $\gamma = 0$, the full lines are calculated with an infinite domain wall energy $\gamma = \infty$ For all temperatures, $|M_{\rm rem}|$ is calculated after $t = 1000$ MCS, starting from the fully aligned state.

by arrow 1), the curves for $\gamma = 0$ and $\gamma = 5.6$ meV start to differ, the latter follow the full lines which is the case for $\gamma = \infty$. Here, the relaxation happens via *coherent rotations* of small island clusters. Above a second temperature (indicated by arrow 2), the remanent magnetizations for finite and infinite γ deviate, since then *internal cluster excitations* become effective. For $K = 0.01$ meV and coverage $\Theta = 0.6$ ML, the difference between the curves for finite and infinite γ is small, thus, here the magnetic relaxation happens mainly via coherent rotation. In contrast, for $K = 0.01$ meV and $\Theta = 0.8$ ML or the larger anisotropy $K = 0.1$ meV, obviously both relaxation channels are effective.

Which relaxation process is effective at a given temperature is determined by its energy barrier ΔE. For a coherent rotation of an isolated island cluster, ΔE is given by its total anisotropy energy $\sum N_i K_i$. In contrast, ΔE for an internal cluster excitation consists of both the anisotropy of the actually reversed islands and the domain wall energy, see Eqs. (3.47) and (3.48). By closer investigation we find that a particular relaxation process becomes effective above a temperature amounting to 5 – 10 % of the respective ΔE. In the temperature ranges $T < 40$ K for $K = 0.01$ meV and $T < 100$ K for $K = 0.1$ meV, each internal cluster excitation consists mainly of reversing only one or two island spins within a single MC update. For markedly higher temperatures, the internal cluster excitations become more complex and depend in a complicated manner on the nanostructure.

5.4.2 Effect of the dipole interaction

In this subsection, the inter-island dipole coupling is included, in addition to the single-island anisotropy and the exchange coupling between connected islands. The influence of this anisotropic long-range interaction on the magnetic relaxation behavior is studied for coverages $\Theta < \Theta_{\mathrm{P}} = 0.9$ ML. We report on results for both cases of the island spin directions, namely *in-plane* magnetizations along the x axis and *out-of-plane* magnetizations along the z axis.

The influence of the dipole coupling on the relaxation of $|M_{\mathrm{rem}}|$ with in-plane island spins S_i^x is shown in Fig. 5.15. Results for two coverages $\Theta < \Theta_{\mathrm{P}}$ are depicted. The open symbols refer to results, already shown in Fig. 5.12 (a), where the dipole coupling has been neglected. The filled symbols denote results, where additionally the dipole coupling is taken into account. We observe that the dipole interaction results in a small *increase* of $|M_{\mathrm{rem}}|$ and T_{b}, which is at the most ~ 10 % for $\Theta = 0.8$ ML. Thus, for *in-plane* island spins the dipole interaction stabilizes the aligned spin state and leads to a somewhat *slower* magnetic relaxation. Surprisingly, this effect is visible in the whole temperature range up to T_{b}, and is *not* limited to those low temperatures where the dipole coupling induces a magnetic ordering with

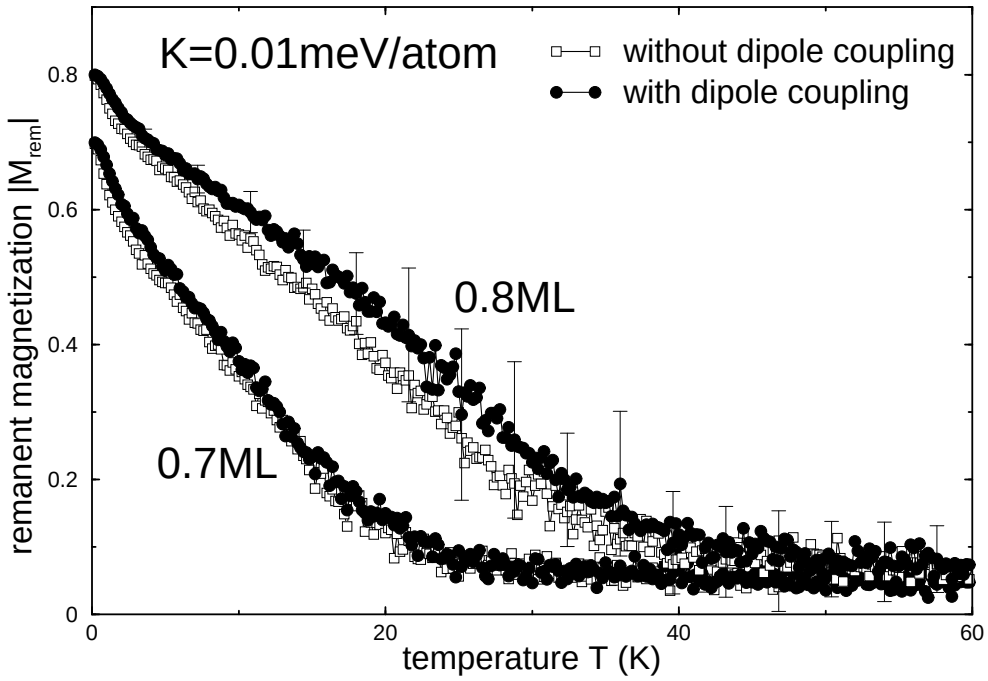

Figure 5.15: Influence of the dipole coupling on the temperature dependence of the remanent magnetization $|M_{\rm rem}|$ as shown in Fig. 5.12 (a). Results for two coverages $\Theta < \Theta_{\rm P} = 0.9$ ML are shown. The dipole interaction leads to a small increase of $|M_{\rm rem}|$ and the blocking temperature $T_{\rm b}$ and thus to a slower relaxation.

$T_{\rm C} \approx 6$ K, see Fig. 5.4.

To investigate the combined effect of the dipole coupling and the single-island anisotropy K in the following, we neglect the inter-island exchange coupling ($\gamma = 0$). As an example, we use the bilayer islands at coverage $\Theta = 2.0$ ML as structural input for the values and locations of the island magnetic moments, and apply the SSF algorithm. Fig. 5.16 shows results for the remanent magnetization $|M_{\rm rem}|$ as function of temperature T. Again, for all temperatures $|M_{\rm rem}|$ is monitored after $t = 1000$ MCS, starting from the fully aligned state. The two different anisotropy values (a) $K = 0.01$ meV, and (b) $K = 0.1$ meV are assumed, leading to different ratios of the dipole energy of an island and the single-island anisotropy. The filled circles indicate a noncoupled (NC) spin system with a vanishing equilibrium magnetization $|M^0_{\rm eq}|$, where the dipole interaction is neglected. Here, the relaxation is only influenced by single-island energy barriers, resulting in $T_{\rm b} \propto K$. For the open squares, the dipole coupling (DC) for in-plane (ip) spins S^x_i is included. The open triangles refer to dipole-coupled (DC) spins S^z_i with easy axes perpendicular (perp) to the surface. The dashed line symbolizes the equilibrium magnetization $|M_{\rm eq}(T)|$ of the in-plane, dipole-coupled spins. Here, the

dipole coupling leads to a long-range magnetic order with ordering temperature $T_C \approx 3$ K.

In Fig. 5.16 (a), the smaller anisotropy $K = 0.01$ meV is assumed. Here, the dipole energy E^i_{dip} of a single island and its anisotropy $K_i N_i$ are obviously of comparable size, since the in-plane, dipole-coupled spins exhibit a long-range order with $T_C \approx 3$ K and the noncoupled system shows a blocking temperature of $T_b \approx 5$ K. Now, we turn to $|M_{\mathrm{rem}}|$ of the dipole-coupled system. For the case of in-plane spins (squares), the dipole coupling strongly prefers an aligned magnetization (ferromagnetic state). Hence, it *slows down* the magnetic relaxation and *increases* the blocking temperature. We explain this behavior as follows: Both, the dipole energy and the anisotropy barriers, stabilize the initial aligned spin state. For the dipole interaction, this is especially true for temperatures $T < T_C$. Nevertheless, for $T > T_C$ this long-range interaction still couples small islands to large islands, which are blocked by anisotropy energy barriers. This leads to an effective increase of T_b. However, for perpendicular spins, the dipole-coupling results in a different behavior. In this case, the dipole energy leads to a long-range *antiferromagnetic* coupling between the spins, see Eq. (3.23). We expect a long-range magnetic order with vanishing net magnetization $|M_{\mathrm{eq}}| = 0$ and an ordering temperature of the same order as calculated for the in-plane case. In other words, the demagnetizing field drives the system towards a zero-net-magnetization, where the magnetic stray field is minimal. Thus, in this case the dipole interaction *accelerates* the magnetic relaxation and *reduces* the blocking temperature T_b.

In Fig. 5.16 (b), we present results for the 10 times larger anisotropy value $K = 0.1$ meV. Correspondingly, for the noncoupled system (NC) the blocking temperature due to anisotropy barriers amounts to $T_b \approx 50$ K. Here, the dipole interaction is weak as compared to the anisotropy, since it leads to low ordering temperatures $T_C \approx 3$ K. Nevertheless, a pronounced effect of the dipole coupling on the temperature dependence of $|M_{\mathrm{rem}}(t = 10^3\,\mathrm{MCS}, T)|$ is visible in the same way as in Fig. 5.16 (a), in particular also for temperatures $T \gg T_C \approx 3$ K.

Recently, Poddar *et al.* observed a similar effect in experiments on magnetic nanoparticles with *random* anisotropy axes [131]. For 2D arrays of separated, dipole-coupled particles, the authors measured higher blocking temperatures T_b than for magnetically isolated particles with the same size distribution. The dependence of this increase of T_b on the distribution of the anisotropy axes and the connection to the case of *uniform* island easy axes, studied in the present thesis, needs for further investigation.

Furthermore, it is very tempting to study the effect of the inter-island dipole coupling and the single-island anisotropy on the relaxation laws of $|M_{\mathrm{rem}}|$ into the collectively ordered states for low temperatures as well as into

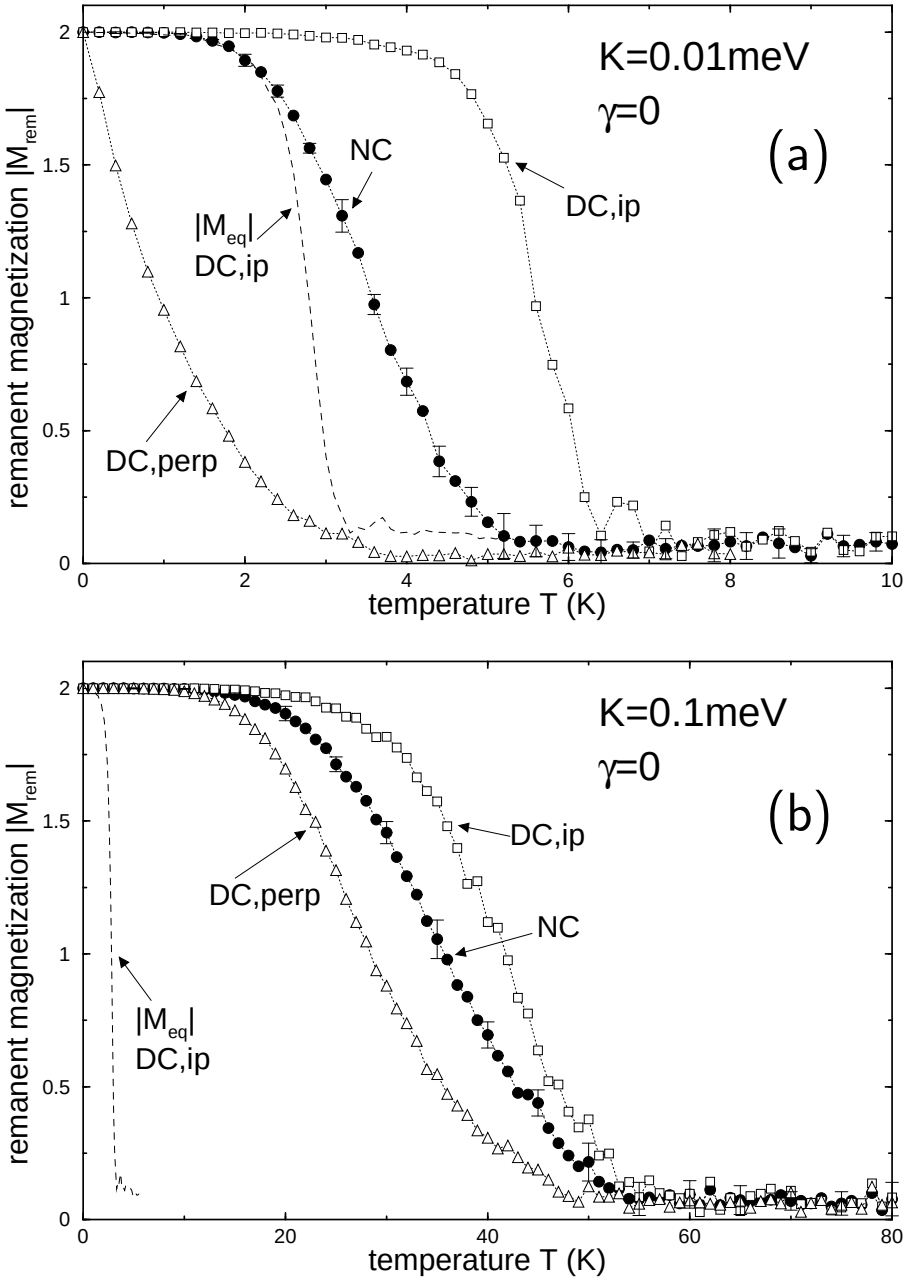

Figure 5.16: The remanent magnetization $|M_{\rm rem}|$ is shown as function of temperature T for two different anisotropy values, (a) $K = 0.01$ meV and (b) $K = 0.1$ meV. For all temperatures $|M_{\rm rem}|$ is calculated after $t = 1000$ MCS, starting from the fully aligned spin state. The filled circles refer to noncoupled island spins (NC). The open squares indicate dipole-coupled (DC) in-plane (ip) spins; the open triangles symbolizes dipole-coupled (DC) perpendicular (perp) spins. The inter-island exchange interaction is neglected ($\gamma = 0$). For comparison, the dashed line refers to the equilibrium magnetization $|M_{\rm eq}|$ of the in-plane, dipole-coupled spins.

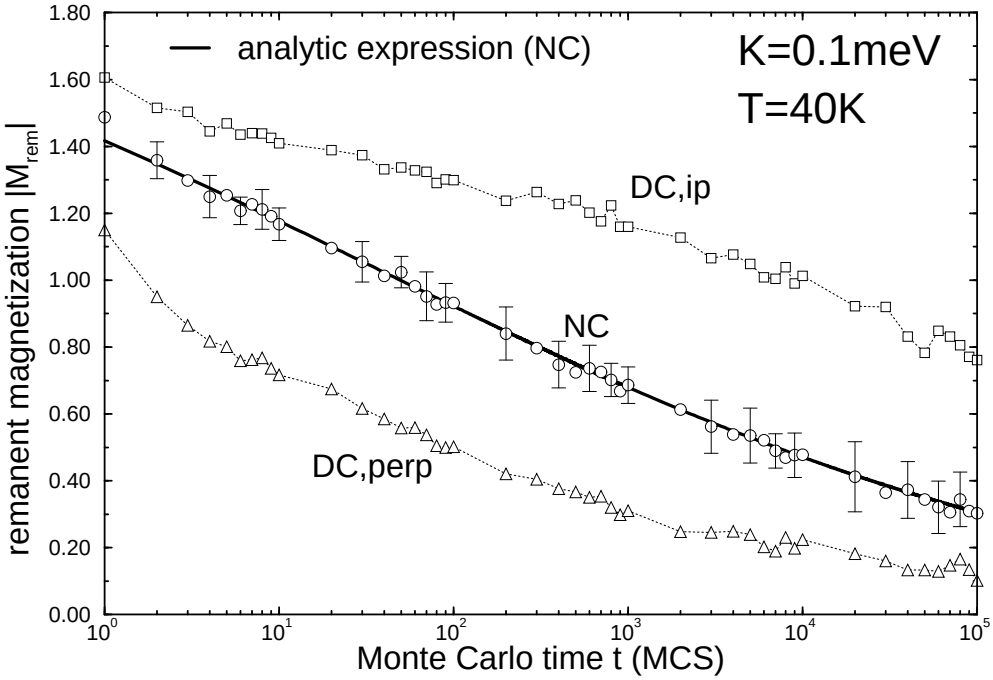

Figure 5.17: The remanent magnetization $|M_{\rm rem}(T,t)|$ is plotted as function of MC time t for temperature $T = 40$ K and anisotropy parameter $K = 0.1$ meV. The solid curve refers to results obtained from Eq. (3.19) for the noncoupled (NC) system. The MC results are indicated by the symbols. Results for noncoupled as well as dipole-coupled (DC) in-plane (ip) and out-of-plane (perp) spins are shown.

disordered (superparamagnetic) states for high temperatures. In Fig. 5.17, the latter case for relaxation into $|M_{\rm eq}| = 0$ is shown. The remanent magnetization $|M_{\rm rem}(T,t)|$ is plotted as function of MC time t for temperature $T = 40$ K, starting from the aligned state. The larger anisotropy value $K = 0.1$ meV, as discussed for Fig. 5.16 (b), is assumed. The solid line refers to results obtained by Eq. (3.19) for the relaxation of an ensemble of noninteracting islands with nonuniform single-island anisotropy barriers $\Delta E_i = N_i K_i$. This slow decay of $|M_{\rm rem}|$ results from an superposition of exponential functions for the time dependencies of the single islands. The circles indicate the corresponding kinetic MC results for the noncoupled system, an excellent agreement with the analytic result is obtained. The squares and triangles refer to results, where the inter-island dipole couplings are included. Here, the dotted lines are guides to the eye. For the perpendicular, dipole-coupled island spins, the initial strong decrease of $|M_{\rm rem}|$ is followed by a slower relaxation, since the driving demagnetizing field becomes smaller.

The determination of the relaxation laws for the interacting island system is an open problem and needs further investigation.

In this context, Lottis *et al.* reported on calculations assuming periodical *uniform* 2D spin systems with uniaxial out-of-plane anisotropy at high temperatures [97]. The dipole interaction between the spins was taken into account within a mean-field approach, leading to a slow *streched-exponential* relaxation of the remanent magnetization from the saturated *out-of-plane* spin state into the disordered state. Recently, a deviating relaxational behavior was calculated by Denisov *et al.* for the same system using an improved numerical method [39]. For *nonuniform* 3D particle systems, Ulrich *et al.* recently found a crossover from a *streched-exponential* to a *power-law* decay of $|M_{\mathrm{rem}}|$ for an increasing strength of the dipole interaction using the MC method [163].

While a number of, sometimes contradictory, experimental and theoretical studies have been reported on 3D nanoparticle systems [5, 57, 86, 100, 41, 53] during the last years, up to now only few studies exist on 2D systems. A detailed investigation of the combined influence of the single-particle anisotropy and the dipole coupling, of the temperature, of the structural disorder (nonuniform particle sizes and easy axes), of the island arrangement (chains etc.), and of noncollinear spin states on the magnetic relaxation of nanoparticle systems is needed. In particular, the crossover from a relaxation behavior determined by *single-island* energy barriers to a *collective* relaxation due to island-island interactions is unclear. These interesting problems remain for future studies.

5.4.3 Coverages above the percolation threshold

In this subsection, we investigate the magnetic relaxation for film coverages Θ above the percolation threshold $\Theta_{\mathrm{P}} = 0.9$ ML of the bilayer island growth mode. The inter-island exchange interaction $\gamma = 5.6$ meV and the single-island anisotropy K are taken into account. The dipole coupling is neglected, since only a very small effect of this weak interaction is expected for systems with a percolating structure, see Sec. 5.3.2.

In Fig. 5.18, the remanent film magnetization $|M_{\mathrm{rem}}(\Theta, T, t)|$ is shown as function of MC time t for coverage $\Theta = 1.0$ ML, slightly above Θ_{P}. The temperature $T = 50$ K is assumed. For vanising anisotropy, $K = 0$, $|M_{\mathrm{rem}}|$ relaxes after $\sim 10^5$ MCS into thermal equilibrium with $|M_{\mathrm{eq}}| \approx 0.35$. As shown in Fig. 5.7, the inter-island exchange coupling induces a long-range ferromagnetic ordering in this system, independent of K. For a finite anisotropy $K = 0.01$ meV the relaxation happens much more slowly due to anisotropy energy barriers; only after 10^6 MCS the curve almost reaches the equilibrium value. For the larger anisotropy $K = 0.1$ meV, the remanent magnetization does not relax into equilibrium within the depicted time range. Thus, we observe that also for coverages $\Theta > \Theta_{\mathrm{P}}$ the magnetic relaxation is strongly influenced by anisotropy barriers.

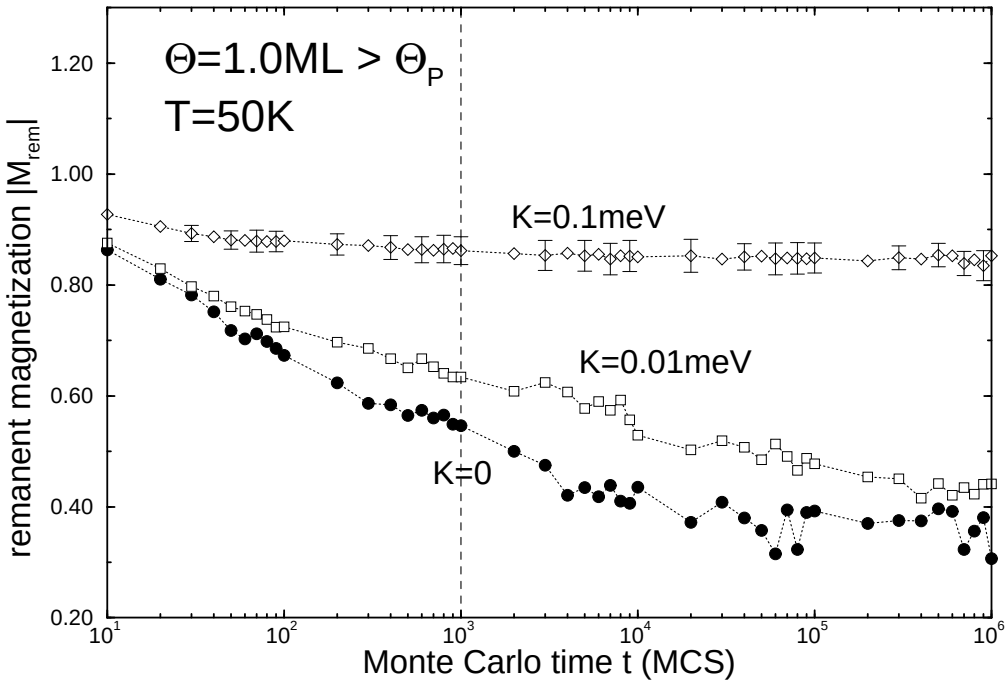

Figure 5.18: Relaxation of the remanent magnetization $|M_{\rm rem}(\Theta, T, t)|$ as function of MC time t for coverage $\Theta = 1.0 > \Theta_{\rm P} = 0.9$ ML. Different anisotropy parameters, $K = 0$, 0.01 and 0.1 meV are taken into account. The inter-island exchange coupling amounts to $\gamma = 5.6$ meV. The dashed line refers to the time $t = 1000$ MCS. The relaxation of $|M_{\rm rem}|$ is strongly hindered by single-island anisotropy barriers.

Next, in Fig. 5.19, the dependency of the influence of anisotropy energy barriers on the coverage of films with percolating structures is investigated. The open symbols show the remanent magnetization $|M_{\rm rem}(\Theta, T, t)|$ as function of temperature T for different coverages Θ. $|M_{\rm rem}|$ is monitored after a waiting time $t = 1000$ MCS, starting from the saturated island spin state. Two different anisotropy values $K = 0.01$ and $K = 0.1$ meV are assumed. For comparison, the equilibrium magnetizations $|M_{\rm eq}(\Theta, T)|$ are depicted by filled symbols. We observe that the blocking temperatures $T_{\rm b}(\Theta)$ are markedly larger than $T_{\rm C}(\Theta)$ in the coverage range $\Theta \gtrsim \Theta_{\rm P}$, where the nanostructure of the percolated thin film is still very irregular, see Fig. 2.6 (e) - (g), p. 30. Here, nonequilibrium effects due to anisotropy barriers are pronounced. For films with larger coverages, having a higher connectivity between islands, the strong exchange coupling results in a fast magnetic relaxation and thus in a smaller temperature difference $T_{\rm b} - T_{\rm C}$. For $\Theta = 1.6$ ML and $K = 0.1$ meV, the remanent magnetization deviates only slightly from $|M_{\rm eq}|$.

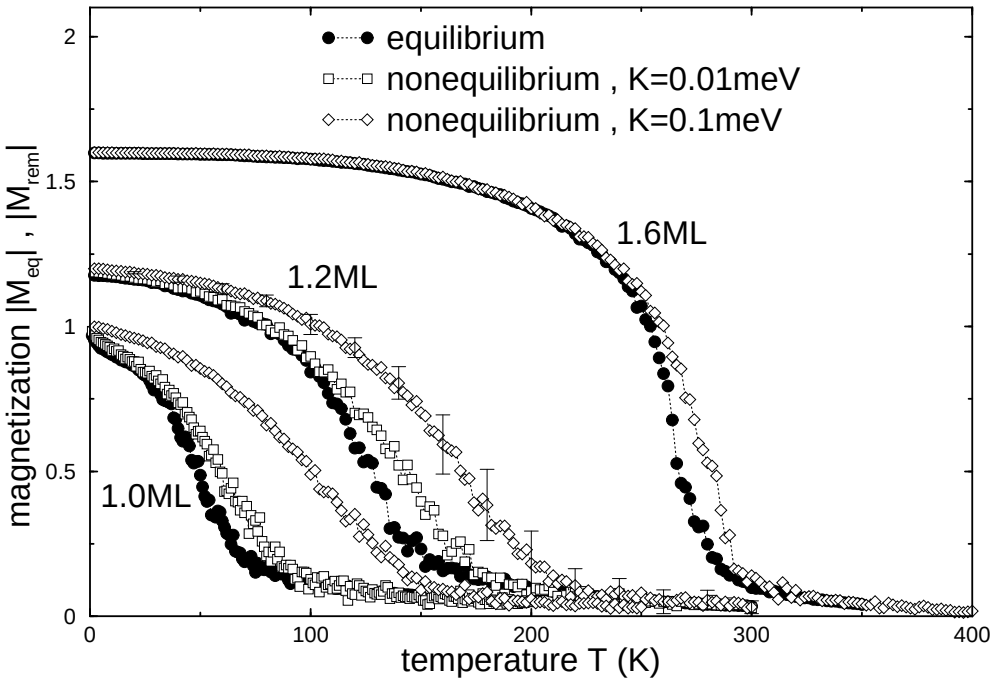

Figure 5.19: The remanent magnetization $|M_{\rm rem}(\Theta, T, t)|$ after $t = 1000$ MCS is shown as function of temperature T for different coverages Θ. For the anisotropy the values $K = 0.01$ and 0.1 meV are assumed. For comparison, the corresponding equilibrium magnetizations $|M_{\rm eq}(\Theta, T)|$ are depicted. The influence of the anisotropy K decreases for increasing coverage.

5.4.4 Summary of the magnetization study

In Fig. 5.20, we present a summary of the most important results on the long-range magnetic ordering and magnetic relaxation of the bilayer island-type film during growth. The (nonequilibrium) blocking temperature $T_{\rm b}(\Theta, K)$ and the (equilibrium) ordering temperature $T_{\rm C}(\Theta)$ are shown as functions of coverage Θ in the whole investigated growth range. For a better visualization, a logarithmic temperature scale is applied. $T_{\rm b}$ is determined for two different anisotropies $K = 0.01$ and 0.1 meV, and a waiting time $t = 1000$ MCS.

Below the percolation coverage $\Theta_{\rm P} = 0.9$ ML, the inter-island dipole coupling induces low ordering temperatures $T_{\rm C}$ of the order of 1 – 10 K for the assumed model parameters. For in-plane island spins S_i^x and $T < T_{\rm C}$, the ordering results in finite net magnetizations. Due to the coagulation of islands with increasing coverage, the inter-island exchange interaction becomes more important, since it couples single islands to magnetically aligned large clusters. This results in a strong increase of $T_{\rm C}$, in particular close to $\Theta_{\rm P}$. This behavior has been observed in experiments on Co/Cu(001) ultrathin films ('$T_{\rm C}$-jump') [17, 133]. For coverages above $\Theta_{\rm P}$, the ordering temperature is

of the order of 100 K – 300 K and is, within the accuracy of our calculations, exclusively determined by the exchange coupling. The slope of $T_{\mathrm{C}}(\Theta)$ for $\Theta > \Theta_{\mathrm{P}}$ is not as steep as for $\Theta < \Theta_{\mathrm{P}}$.

The nonequilibrium behavior, as caused by the single-island magnetic anisotropy K, differs strongly for coverages Θ below and above Θ_{P}. Here, a waiting time $t = 1000$ MCS is assumed. For $\Theta < \Theta_{\mathrm{P}}$, a blocking temperature $T_{\mathrm{b}}(\Theta)$ is obtained which is an order of magnitude higher than $T_{\mathrm{C}}(\Theta)$ resulting from the dipole interaction. Evidently, T_{b} depends on the anisotropy K. A simple proportionality $T_{\mathrm{b}} \propto K$ is not present, due to relaxation via internal island cluster excitations besides coherent cluster rotations. The dipole coupling between islands somewhat slows down the magnetic relaxation in the case of in-plane island spins S_i^x. However, for out-of-plane spins S_i^z we find an acceleration of the relaxation due to this coupling. For the bilayer island growth mode this effect is small, but can become larger for increased dipole energies in respect to the single-island anisotropy barriers. On the other hand, for $\Theta > \Theta_{\mathrm{P}}$, the relaxation into ferromagnetically ordered island spin states is accelerated by the inter-island exchange coupling. For increasing Θ, the remanent magnetization reaches the equilibrium value within the assumed waiting time $t = 1000$ MCS, and $T_{\mathrm{b}}(\Theta)$ merges into $T_{\mathrm{C}}(\Theta)$.

Next, we discuss our results in connection with measurements on Co-/Cu(001) ultrathin films, see Fig. 1.2, p. 15. Although several model parameters are chosen in accordance with this system, a full quantitative comparison cannot be drawn yet. The main reason is that the observed intermixing of Co adatoms with Cu substrate atoms is not taken into account properly within our simple growth model due to the incomplete knowledge of the resulting atomic morphology (Co island sizes, positions, etc.), as mentioned on p. 35. The measured percolation threshold $\Theta_{\mathrm{P}}^{\mathrm{exp}} \approx 1.7$ ML is much larger than the threshold $\Theta_{\mathrm{P}} = 0.9$ ML of our model system. Also, the morphology of the Co film can be much different at coverages close to $\Theta_{\mathrm{P}}^{\mathrm{exp}}$.

To investigate solely the effect of an enlarged Θ_{P}, we have performed additional simulations simply by taking into account magnetic islands with up to *three* atomic layers, yielding the observed $\Theta_{\mathrm{P}}^{\mathrm{exp}} \approx 1.7$ ML. Then, for a coverage $\Theta = 1.6$ ML, the dipole coupling induces an ordering temperature $T_{\mathrm{C}} \approx 50$ K due to large island magnetic moments. The corresponding blocking temperature for $K = 0.01$ meV and waiting time $t = 1000$ MCS is obtained to be $T_{\mathrm{b}} \approx 150$ K. These temperatures are comparable with the measurements which observe for coverages slightly below $\Theta_{\mathrm{P}}^{\mathrm{exp}}$ a remanent magnetization for temperatures up to $T \approx 150$ K [17].

Thus, we find that for the assumed growth modes and magnetic parameters, the blocking temperatures T_{b} are always markedly higher than the ordering temperatures T_{c}. We point out that in this case it might be practically impossible to observe the ordered low-temperature phase when starting

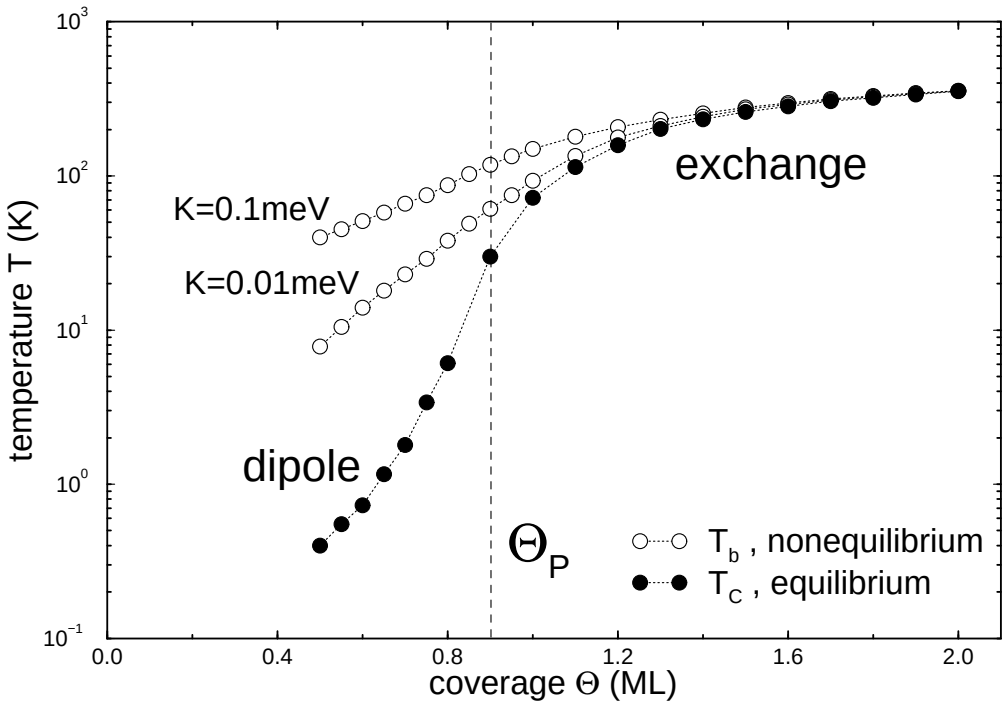

Figure 5.20: Semi-logarithmic plot of the magnetic ordering temperature $T_{\mathrm{C}}(\Theta)$ and the blocking temperature $T_{\mathrm{b}}(\Theta)$ as functions of the film coverage Θ using the bilayer growth mode. The temperatures T_{C} and T_{b} are extracted from the preceding figures. The entire investigated coverage range below and above the percolation coverage $\Theta_{\mathrm{P}} = 0.9$ ML is shown. The different magnetic interactions exhibit a varying influence at different coverages, as indicated. For $\Theta < \Theta_{\mathrm{P}}$, the dipole interaction causes a long-range magnetic ordering with small T_{C}. Approaching Θ_{P}, the exchange interaction induces a strong increase of T_{C}. The nonequilibrium behavior is governed mainly by the anisotropy. For $\Theta > \Theta_{\mathrm{P}}$ the exchange interaction dominates.

from a saturated magnetization, since then the magnetic relaxation into equilibrium is strongly hindered by anisotropy energy barriers.

In addition, to draw a quantitative comparison with the Co/Cu(001) thin film system, a *four-fold* symmetry of the in-plane anisotropy has to be taken into account. Nevertheless, we expect that the above stated general behavior of the long-range magnetic ordering and magnetic relaxation, obtained with a uniaxial anisotropy, will not be changed. Furthermore, in our study, we have assumed site-independent parameters J, K, and μ_{at}. Due to variations of the electronic structure, however, these values may vary considerably, in particular for adatoms close to the interface, at island edges, etc. Large variations have been observed and calculated, e. g. for Fe thin films on W [15, 123, 134]. Also the domain wall energy (inter-island exchange coupling) γ may depend on the nanostructure [24].

Finally, we wish to point out recent experiments on ultrathin Co/Cu(110) systems, performed by Bland and co-workers [67]. STM measurements revealed that here Co grows via the formation of large, elongated, 3D islands, resulting in an in-plane uniaxial (shape) anisotropy of the magnetization direction. The authors observed an onset of *room*-temperature ferromagnetism at a critical coverage of $\Theta_{\mathrm{c}} \approx 4.6$ ML, and attributed it to a percolation phase transition and the exchange interaction between coalesced islands. Possibly, ultrathin Co/Cu(110) is a suited experimental model system with uniaxial magnetic anisotropy for the study of magnetic ordering and relaxation dependent on the coverage, as investigated in the present thesis. In particular, it would be interesting to have experimental results for the magnetic behavior at coverages $\Theta < \Theta_{\mathrm{c}}$ and at *low* temperatures, where a long-range ordering with finite net magnetization due to inter-island dipole couplings might be found.

5.5 Metastable magnetic domain structure

In this section, we present results of the 'as-grown' metastable magnetic domain structure, obtained from kinetic MC simulations. The bilayer island growth mode (version II) is used as structural input. The inter-island exchange coupling $\gamma = 5.8$ meV and the single-island anisotropy $K = 0.2$ meV are taken into account. The dipole coupling is neglected. Snapshots of domain structures are shown and discussed. Results for the average domain area $\overline{A}(\Theta, T)$ and the average domain roughness $\overline{r}(\Theta, T)$ are presented, dependent on the film coverage Θ and the temperature T during growth. The role of nonuniform inter-island exchange couplings for the collective magnetic relaxational behavior and the metastable domain formation is studied.

The magnetic relaxation and the film growth happen simultaneously after starting from a random island spin state, according to the scheme given in

p. 62. If not otherwise stated, exclusively the SSF algorithm and the adatom deposition rate 1 ML/100 sec are applied to the kinetic MC simulations.

5.5.1 Snapshots of domain structures

In Fig. 5.21, we show snapshots of resulting magnetic domain structures for different film coverages Θ. The systems were grown at temperature $T = 100$ K. For small coverages, (a), the domain area resembles the island area. For large coverages $\Theta \lesssim 2$ ML, (d), the thin film is almost closed and consequently the ferromagnetic domains are very large. Very interestingly, for coverages near and above the percolation threshold $\Theta_{\mathrm{P}} = 0.9$ ML, (b) and (c), the domains adopt an intermediate size, covering several neighboring islands. These irregular 'as-grown' domains correspond to metastable island spin states far from thermodynamical equilibrium, since the equilibrium state is represented by a ferromagnetic alignment, see results of Sec. 5.3.2. We claim that this micro-domain structure is controlled and stabilized by the *nonuniform* nanostructure of the growing ultrathin film which results in nonuniform inter-island exchange couplings $L_{ij}\,\gamma_{ij}$ and single-island anisotropies $N_i\,K_i$. Such a *random* ferromagnetic system can be easily trapped in metastable states with a frozen-in domain structure with an average domain size between the above mentioned extremal sizes. The influence of the nonuniform inter-island couplings on the metastable domain structure is investigated in Sec. 5.5.4. We suggest that the experimentally observed small 'as-grown' magnetic domains in Co/Au(111) ultrathin films with rough morphologies [3, 2, 154, 73], Figs. 1.3 and 1.4, p. 19, are such metastable, nonequilibrium magnetic structures.

The influence of temperature T during growth on the resulting metastable domain structures can be observed in Fig. 5.22. Snapshots of magnetic structures of films at coverage $\Theta = 1.2$ ML and grown at different T are presented. At low temperature $T = 5$ K, small domains with very irregular shapes are obtained. For $T = 30$ K the domains are larger. For $T = 150$ K many small domains are obtained within a few large domains.

To investigate the 'as-grown' metastable magnetic domain structures in more detail, we present in the following two subsections results on the average domain area $\overline{A}(\Theta, T)$ and average domain roughness $\overline{r}(\Theta, T)$ as functions of film coverage Θ and growth temperature T. The domain analysis is performed using the Hoshen-Kopelman algorithm [68] for identifying different magnetic domains, see Appendix C. We note that the mentioned average values represent a rough measure for the strongly nonuniform domain structure and broad distributions of domain areas and roughnesses, in particular for situations depicted in Fig. 5.22 (c). Therefore, large errorbars for $\overline{A}$ and $\overline{r}$ are obtained by the averaging procedure over the broad distribution.

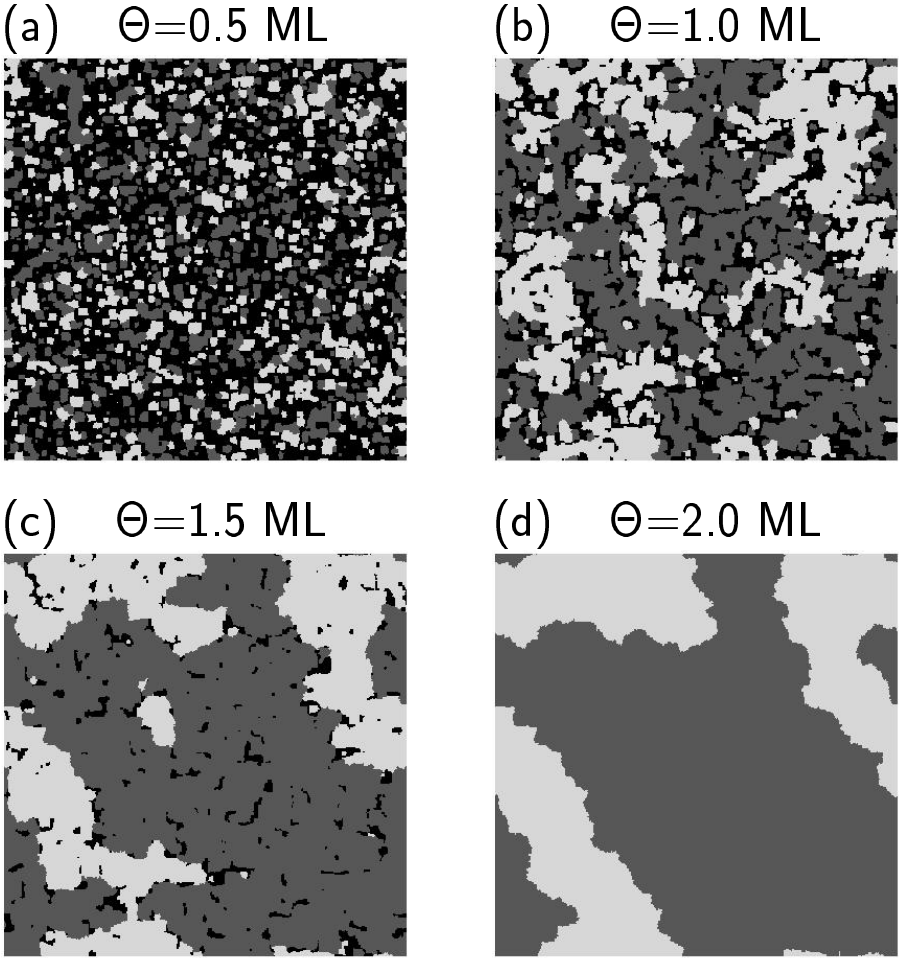

Figure 5.21: Snapshots of magnetic domain structures grown at temperature $T = 100$ K for different coverages (a) $\Theta = 0.5$ ML, (b) $\Theta = 1.0$ ML, (c) $\Theta = 1.5$ ML, and (d) $\Theta = 2.0$ ML. The unit cell has 500×500 lattice sites and contains 1250 islands (island density 0.005 islands per site). Only the domain pattern of the first magnetic layer is shown. The two gray scales refer to the two magnetic directions, the uncovered substrate is black.

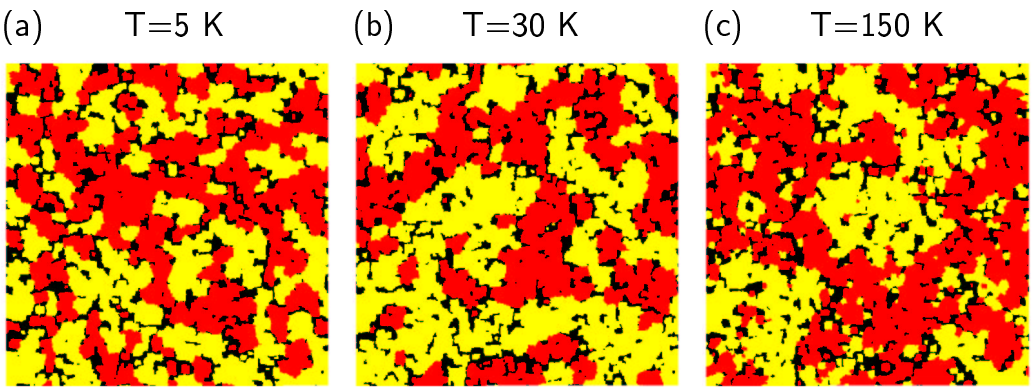

Figure 5.22: Influence of temperature T during growth on the resulting magnetic domain pattern. Snapshots of domain structures at film coverage $\Theta = 1.2$ ML and different T are depicted. The two gray scales refer to the two magnetic directions, black to the uncovered substrate.

5.5.2 Analysis of the average domain area

In Fig. 5.23, results for the average domain area $\overline{A}(\Theta, T)$ in units of lattice sites are shown as function of the film coverage Θ and for different temperatures T during growth. The average single island area $\overline{A}_{\rm is}$ and the average area of islands clusters, which serve as lower and upper limits of $\overline{A}$, are also shown. For coverages well below the percolation threshold $\Theta_{\rm P} = 0.9$ ML the average domain area is of the order of $\overline{A}_{\rm is}$, see Fig. 5.21 (a). In this case, the ultrathin film consists of magnetically almost isolated islands, the exchange coupling between neighboring islands has no large influence. If no additional long range magnetic interactions such as the dipole coupling or the indirect exchange (RKKY-) coupling are important, the system of isolated magnetic islands refers to a superparamagnet. Due to their small size and their superparamagnetic behavior the magnetic domains in this coverage range might be hardly visible with experimental means.

With increasing Θ, the islands start to merge and form large connected island clusters. Caused by the nonuniform island ensemble, the island coalescence does not occur simultaneously in the system. In this coverage region, the average domain area increases considerably, but is still markedly affected by the atomic nanostructure of the thin film, see Fig. 5.21 (b) and (c). We find an average domain area much larger than the average single island area, but still definitely smaller than the area of connected islands.

With further adatom deposition a smooth magnetic thin film is obtained, and the domain pattern is mainly determined by competing magnetic interactions (exchange, anisotropies). Due to the disappearance of small domains, see Fig. 5.21 (d), the *average* domain area becomes very large. Since the ex-

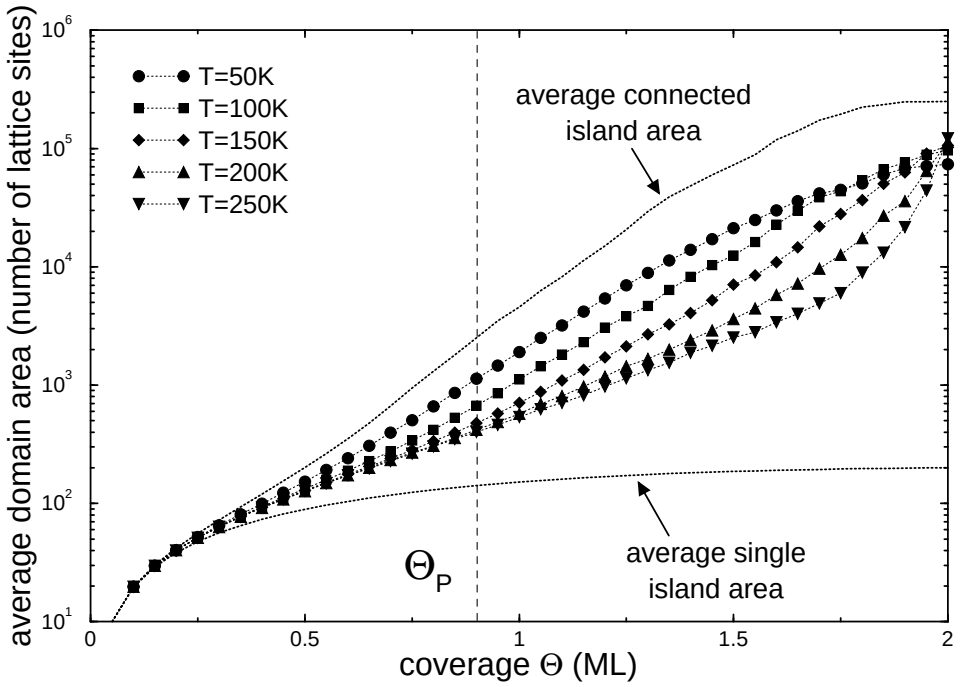

Figure 5.23: Semi-logarithmic plot of the average domain area $\overline{A}(\Theta, T)$ as function of the film coverage Θ for different temperatures T during growth. The dotted lines refer to the average single island area and the average area of connected islands (island clusters) which are the lower and upper limits of $\overline{A}$. The percolation threshold $\Theta_{\mathrm{P}} = 0.9$ ML is indicated by the dahed line.

tension of these large domains reaches the size of our unit cell, we emphasize that in the coverage range of about $1.8 - 2$ ML our simulation of the domain structure is influenced by finite size effects. Besides this, the micromagnetic model should not be applied for a smooth film, since it applies nonuniform island sizes N_i and inter-island exchange couplings $L_{ij}\gamma_{ij}$ which represent an unphysical discretization of uniform systems, see discussion in Sec. 3.3, p. 47.

In Fig. 5.23, larger average domain areas $\overline{A}(\Theta)$ are obtained for lower growth temperatures. To study the influence of the temperature T during domain formation, we present in Fig. 5.24 results for $\overline{A}(\Theta, T)$ as function of T for different film coverages Θ. The island systems are grown at constant temperature, $\overline{A}$ is monitored at the indicated coverages. The curves end roughly at the corresponding ordering temperatures $T_{\mathrm{C}}(\Theta)$. All $\overline{A}(T)$-curves show maxima, in particular at low T. This behavior can also be observed in the snapshots of Fig. 5.22. The reason for this property is that for low temperatures the formation of large, energetically favored, ferromagnetic domains is hindered by energy barriers of the rough energy landscape of the interacting, irregular island system. Since with an increasing T the probability to

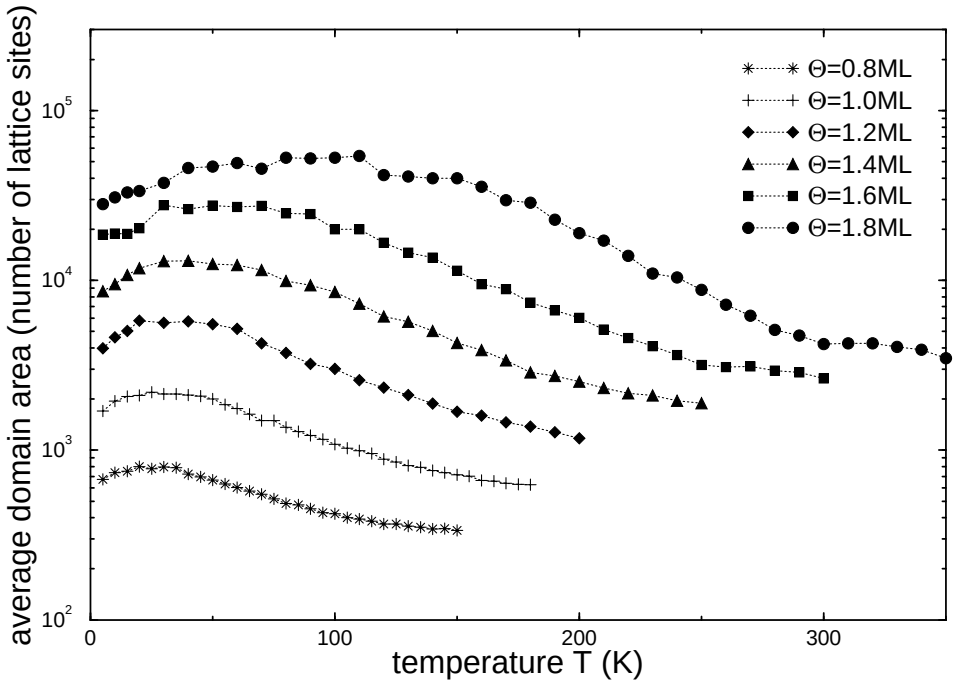

Figure 5.24: Influence of the temperature during growth on the average domain area. A semi-logarithmic plot of the average domain area $\overline{A}(\Theta, T)$ as function of the temperature T for different coverages Θ is shown. The curves end roughly at the corresponding ordering temperatures $T_{\mathrm{C}}(\Theta)$.

overcome energy barriers becomes larger, an increasing average domain area is obtained for larger T. On the other hand, at elevated temperatures, large metastable domains may disintegrate into smaller domains due to thermal agitation, which results in a decreasing average domain area with increasing temperatures. Consequently, while approaching the corresponding Curie temperature $T \rightarrow T_{\mathrm{C}}(\Theta)$ of the long-range ferromagnetic order, the average domain area drops considerably. With an increasing coverage Θ the maximum of $\overline{A}(T)$ is shifted to higher temperatures, since the increasing average magnetic energy between the islands is better suited to withstand thermal agitations.

In the remainder of this subsection, we investigate the influences on $\overline{A}(\Theta, T)$ resulting from the adatom deposition rate, from the applied algorithm, and from single-island anisotropy energy barriers.

The influence of the adatom deposition rate is studied in Fig. 5.25. The average domain area $\overline{A}(\Theta, T)$ is plotted as function of temperature T for film coverage $\Theta = 1.2$ ML and two different deposition rates, 1 ML/100 sec and 1 ML/10000 sec. We observe that the two data sets differ only slightly. The lower deposition rate leads to somewhat larger domain areas for low

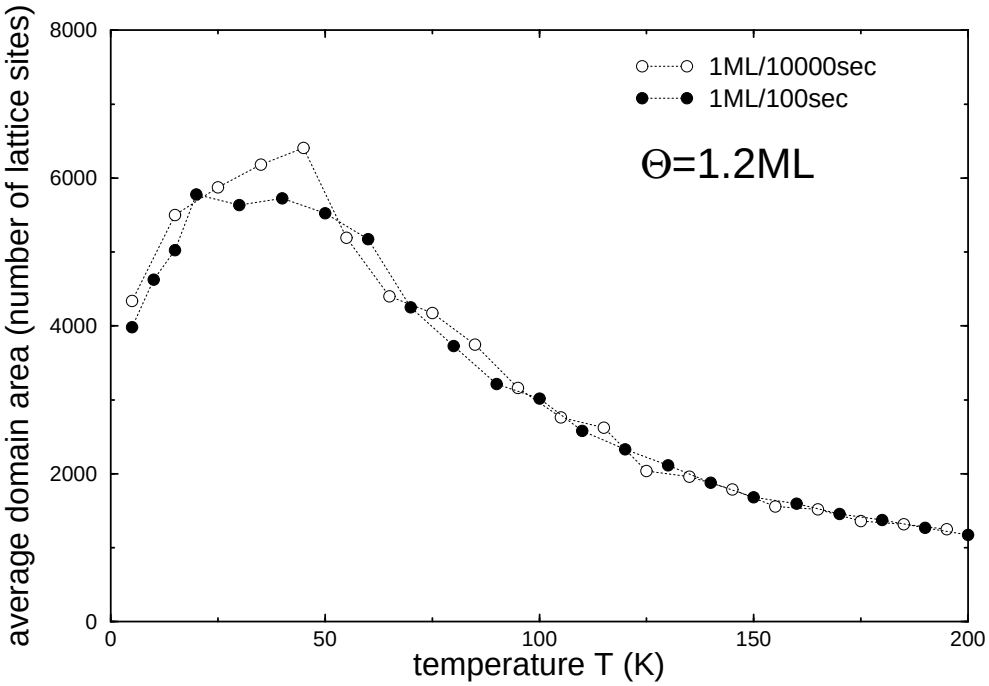

Figure 5.25: Influence of the adatom deposition rate on the magnetic domain structure. The average domain area $\overline{A}(T)$ is plotted as function of temperature T for the coverage $\Theta = 1.2$ ML and two different deposition rates, 1 ML/10000 sec and 1 ML/100 sec.

and intermediate temperatures, where the domain formation is governed by energy barriers. This results from the fact that here the system has more time to relax towards energetically more favorable magnetic structures with larger domains. We conclude that the deposition rate has only a minor influence on the magnetic domain structure due to the strong temporal stability of the metastable magnetic states.

In Fig. 5.26 (a), we compare results obtained by the single-spin-flip (SSF) and the cluster-spin-flip (CSF) MC algorithm. Again, the average domain area $\overline{A}(\Theta, T)$ is plotted as function of temperature T for different coverages Θ. Within the CSF algorithm, the maximum island cluster size $\lambda_{\max} = 8$ is applied. By use of CSF somewhat larger $\overline{A}$ are obtained, in particular at large Θ and small T. This is due to the fact that CSF occasionally facilitates the surmount of energy barriers which are caused by irregular inter-island couplings. We observed that larger $\lambda_{\max}$ do not change the obtained $\overline{A}$, since the magnetic rotation of large island clusters is strongly hindered by the corresponding large total anisotropy barriers. Thus, qualitatively the same behavior of $\overline{A}(T)$, in particular the appearance of maxima, is obtained by SSF and CSF.

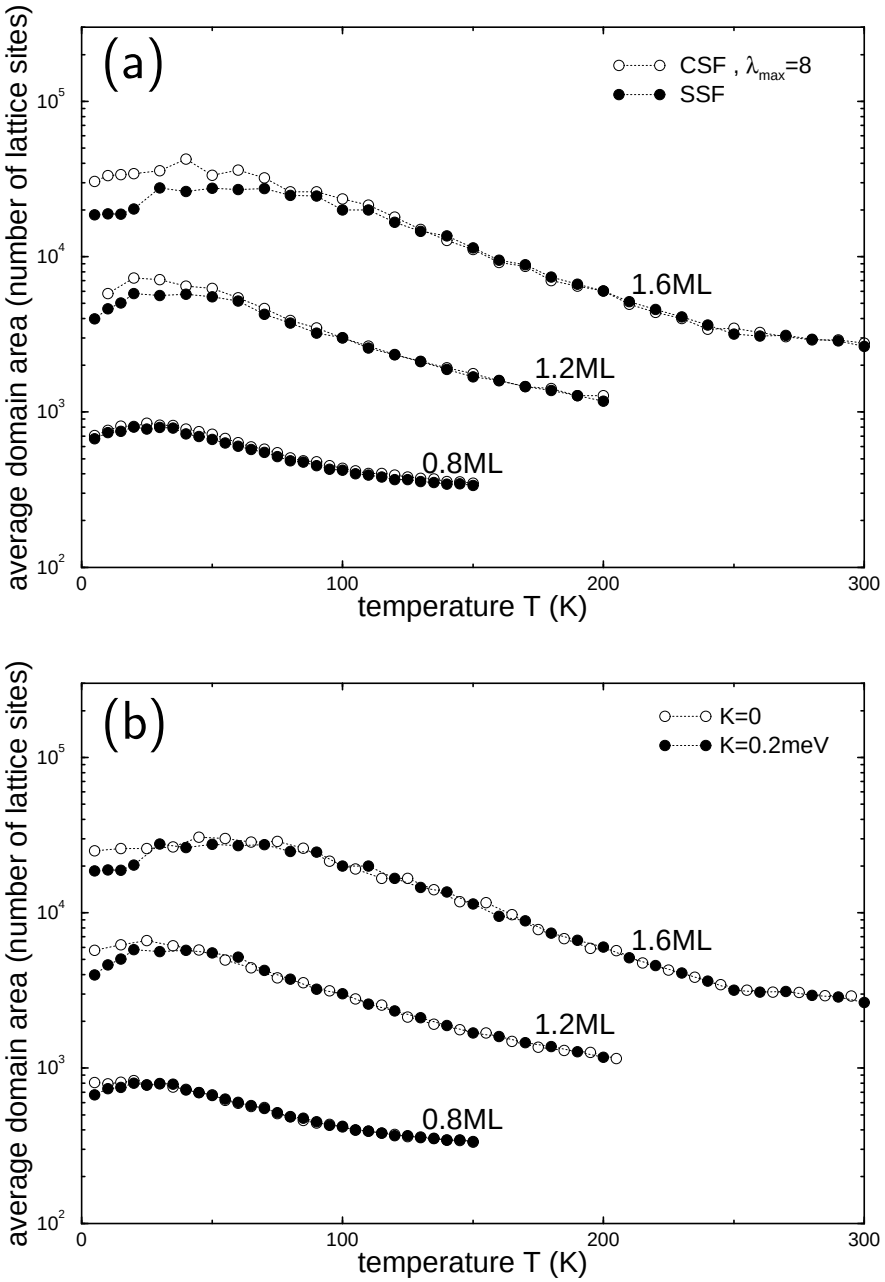

Figure 5.26: Semi-logarithmic plot of the average domain area $\overline{A}(\Theta, T)$ as function of temperature T for different coverages Θ. (a) Results obtained by the single-spin-flip (SSF) algorithm and the cluster-spin-flip (CSF) algorithm with maximum cluster size $\lambda_{\max} = 8$ for coherent island spin rotations are depicted. Only a small difference is seen. (b) Results for a vanishing single-island anisotropy $K = 0$ and for $K = 0.2$ meV are shown. A small influence of K is observed for low temperatures.

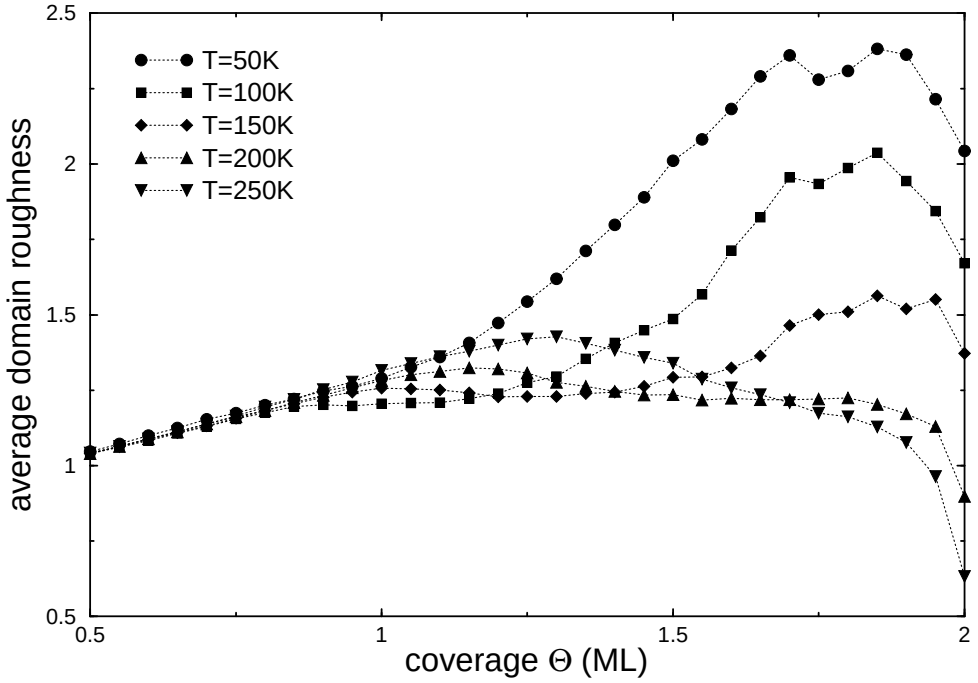

Figure 5.27: Average relative domain roughness $\overline{r} = \overline{R/R_\circ}$ as function of the coverage Θ for different temperatures T during growth. The domain roughnesses are given relative to the minimal roughness $R_\circ$ of circularly shaped domains with the same area. Values $\overline{r} < 1$ result from single-domain samples.

The effect of the single-island anisotropy K on the metastable magnetic domain structure is shown in Fig. 5.26 (b). The average domain area $\overline{A}$ is shown as function of temperature T for different coverages Θ. Additionally to the results obtained for $K = 0.2$ meV, results for $K = 0$ are plotted. We observe that only at low temperatures the formation of large ferromagnetic domains is slightly hindered by anisotropy barriers. We conclude that the metastable domain structure is mainly determined by the *collective* behavior resulting from the irregular inter-island exchange couplings.

5.5.3 Analysis of the average domain roughness

In Fig. 5.27, we present results for the average domain roughness $\overline{r}(\Theta, T)$ as function of the coverage Θ and for different temperatures T during growth. The domain roughness is defined by the edge-to-area ratio of the domains. We present results for the *relative* domain roughness $\overline{r} = \overline{R/R_\circ}$ with respect to the minimal roughness $R_\circ$ of circularly shaped domains with the same area, as described in Sec. 5.1. Values $\overline{r} < 1$ result from single-domain systems due to the averaging procedure. Evidently, there is a pronounced dependency of the

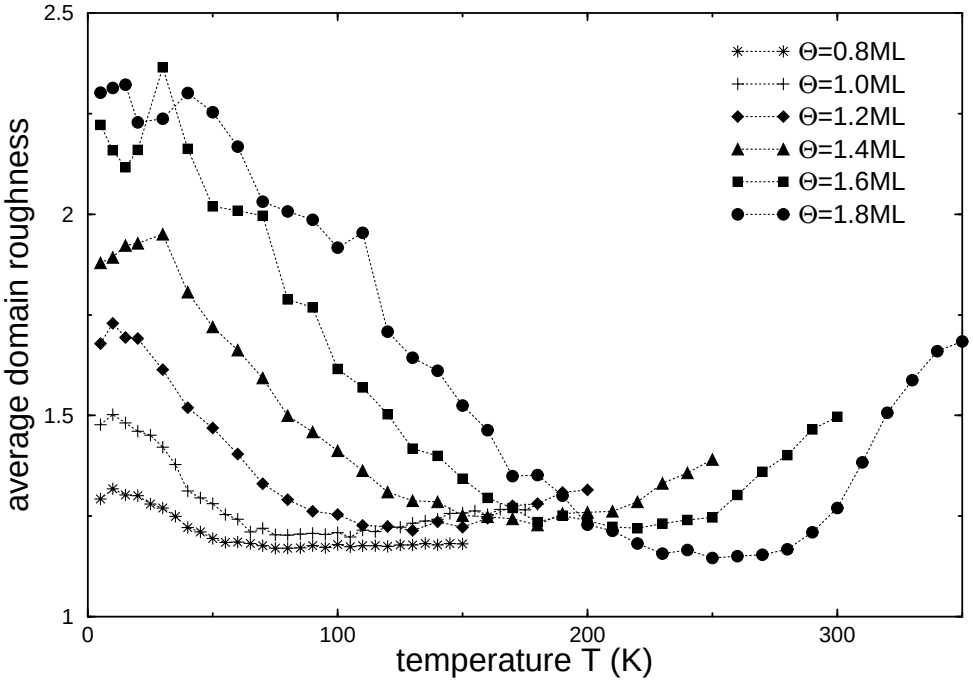

Figure 5.28: Influence of the temperature during growth on the average domain roughness. The average domain roughness $\overline{r}(\Theta, T)$ is plotted as function of temperature T for different coverages Θ. The curves end roughly at the corresponding ordering temperatures Θ_C.

relative domain roughness on Θ and T. For low coverages, larger roughnesses are obtained for higher T. However, for increasing Θ the opposite behavior is observed: an increasing temperature tends to smoothen the domains. As a consequence, the curves for different temperatures do intersect.

The influence of the temperature during growth on the average domain roughness is better seen in Fig. 5.28. Here, the average domain roughness $\overline{r}(\Theta, T)$ is plotted as function of temperature T for different coverages Θ. The island systems are grown at constant temperature, $\overline{A}$ is monitored at the indicated coverages. Similarly as discussed for the average domain area $\overline{A}(T)$, for low T, the formation of energetically favorable smooth domain shapes is hindered by energy barriers of the interacting irregular island system. However, an increasing T facilitates the surmount of the barriers, and the domains may assume more compact shapes, i. e. are less rough. In contrast, an even higher temperature destroys ferromagnetically ordered domains, in particular at their surfaces, thus increasing again the surface-to-area ratio. Consequently, a minimum of $\overline{r}$ as function of T is observed. For increasing coverages, the minimum moves to higher temperatures due to the larger connectivity between the islands. This explains the intersections of curves

in Fig. 5.27. Additional calculations revealed that there is only a very weak dependence of $\overline{r}(\Theta, T)$ on the adatom deposition rate (growth velocity), the applied MC algorithm, and the single-island anisotropy K. We conclude that the domain roughness is mainly governed by the coverage-dependent irregular connectivity of the island system, the inter-island exchange interaction, and the temperature during the domain formation.

5.5.4 Role of nonuniform inter-island couplings

In this subsection, we study the effect of *nonuniform* ferromagnetic inter-island exchange couplings $L_{ij}\gamma_{ij}$ on the formation of metastable magnetic states and draw an analogy to the magnetic 'as-grown' domain structure of irregularly connected island-type films.

For comparison with the previous results, we consider a simplified island spin system. We simulate spins on a regular (34×34)-square lattice with periodic boundary conditions. Thus, every spin has four next neighbors. For the inter-island exchange coupling and the single-island anisotropy we apply the same parameters $\gamma = 5.8$ meV and $K = 0.2$ meV, as used above. We assume for *all* spins the average island size $\overline{N}(1.15\,\mathrm{ML}) = 230$ of the bilayer island growth mode at coverage $\Theta = 1.15$ ML, where the islands are also in average connected to four neighboring islands, see Fig. 2.8, p. 32.

For the island-island bond lengths L_{ij}, we investigate the effect of δ-distributions, centered at L_{ij}^0, and Gaussian distributions

$$\mathcal{P}(L_{ij}) = \frac{1}{\sigma\sqrt{2\pi}} \exp\left(\frac{(L_{ij} - L_{ij}^0)^2}{2\sigma^2}\right) \quad , \tag{5.3}$$

where σ is the standard deviation, determining the width of the distribution, and where L_{ij}^0 is the mean value. The tails of $\mathcal{P}(L_{ij})$ are cut off to allow only for positive values L_{ij}. For the generation of random numbers following a Gaussian distribution, the Box-Muller algorithm is used [146]. We use $L_{ij}^0 = \overline{L_{ij}}(1.15\,\mathrm{ML}) = 13$, which is the average value of the bilayer island growth mode at coverage $\Theta = 1.15$ ML, see Fig. 2.8, p. 32.

We perform MC simulations of the magnetic relaxation of such system, starting from random spin states ('hot start'), and analyse the average magnetic domain area (in numbers of spins) $\overline{A}(t)$ as function of MC time t. The results are averaged over 50 different realizations of the nonuniform distributions $\mathcal{P}(L_{ij})$. In Fig. 5.29 (a), we present results for $\overline{A}(t)$ obtained at temperature $T = 50$ K. Results for uniform couplings (δ-distribution) $L_{ij} = 13$ are indicated by the filled symbols. Here, we observe a fast increase of the average domain area during the MC process. Within the individual MC runs, not always the single-domain state is reached. However, couplings following Gaussian distributions $\mathcal{P}(L_{ij})$, centered at $L_{ij}^0 = 13$, lead to a different behavior, as indicated by the open symbols: the larger the relative

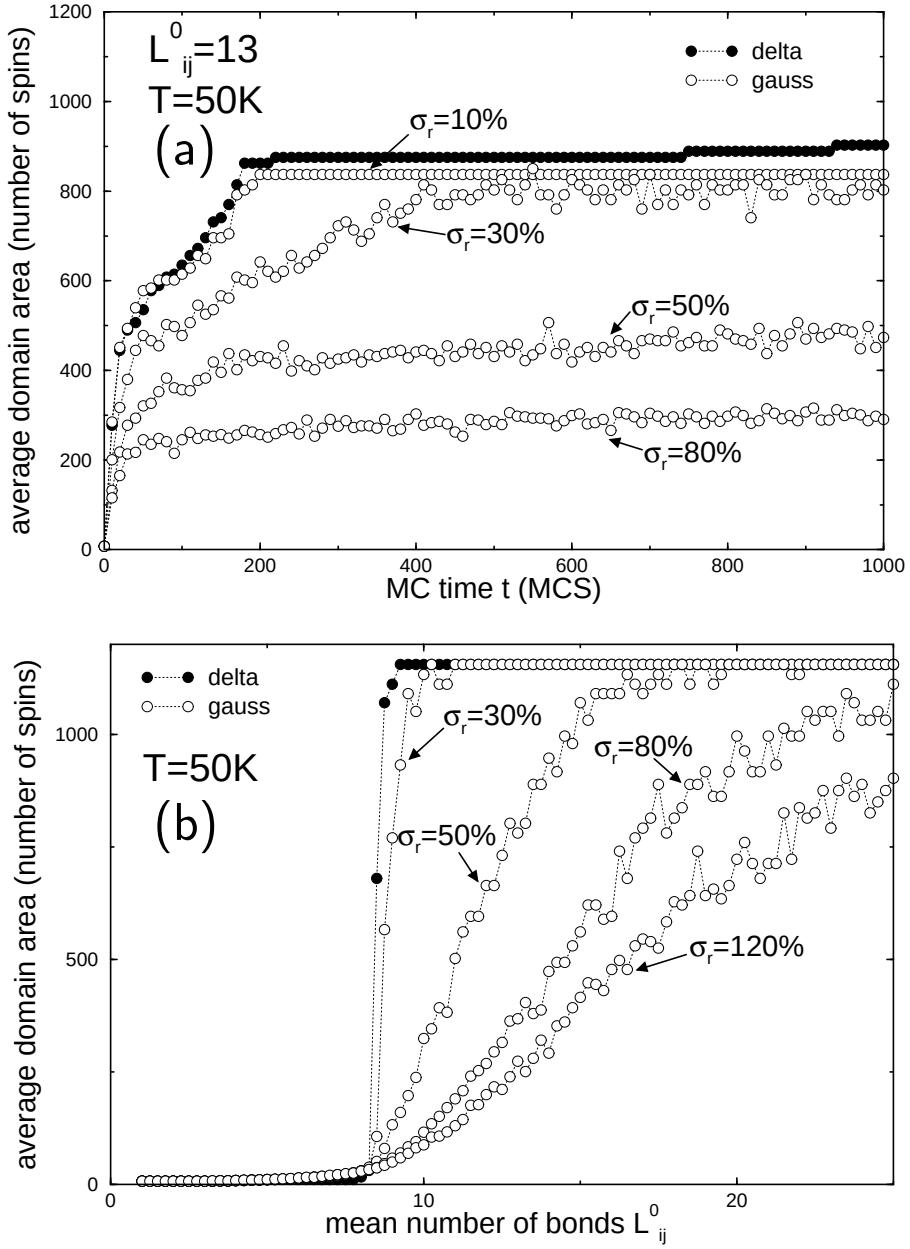

Figure 5.29: Influence of nonuniform inter-island exchange couplings on the domain kinetics within a square lattice of spins, starting from a random spin state. Results for δ-distributions ($\bullet$) and Gaussian distributions ($\circ$) of numbers of atomic bonds L_{ij} between connected islands, centered at L_{ij}^0, are shown. Different relative standard deviations $\sigma_\mathrm{r} = \sigma / L_{ij}^0$ are assumed. (a) The average domain area $\overline{A}(t)$ is plotted as function of MC time t, $L_{ij}^0 = 13$ is used. (b) The average domain area $\overline{A}$ is plotted as function of the mean number of atomic bonds L_{ij}^0, which increases linearly in time during the magnetic relaxation.

standard deviation $\sigma_r = \sigma / L_{ij}^0$ of the distribution, the slower the growth of the ferromagnetic domains. For large σ_r, the systems practically end up in metastable multi-domain states. We conclude, that broad distributions of *nonuniform* couplings between the spins drastically *delay* the formation of large ferromagnetic domains, when starting from a random spin state.

To mimic growing island-type systems, where the number of atomic bonds $L_{ij}(\Theta)$ between the islands increases for increasing film coverage Θ, we performed additional calculations for the square lattice of spins. For the results presented in Fig. 5.29 (b), the mean value L_{ij}^0 of the distributions $\mathcal{P}(L_{ij})$ increases *during* the magnetic relaxation of the spin systems (the growth velocity of L_{ij}^0 amounts to 1 atomic bond/2000 sec). Again, the MC runs are started from random spin states. Here, the average domain area $\overline{A}$ is shown as function of the mean number of atomic bonds L_{ij}^0. For the uniformly coupled spin system, a steep rise of $\overline{A}$ is obtained at a critical value for L_{ij}^0, which corresponds to the onset of a long-range ferromagnetic order at $T = 50$ K. However, for the nonuniform distributions, a much slower increase of $\overline{A}$ is obtained. We suggest that this behavior resembles the behavior of the average domain area $\overline{A}(\Theta)$ of the growing bilayer island system, shown in Fig. 5.23.

In the following, we discuss the results of this subsection. Due to the irregularly connected atomic structures of the investigated bilayer island ensembles, the interfaces L_{ij} between coagulated islands differ considerably, resulting in strongly nonuniform inter-island exchange interactions $L_{ij}\,\gamma_{ij}$. Such a distribution of interactions can be attributed for by a random exchange coupling between neighboring island spins as investigated in this subsection. Thus, irregularly connected island-type film systems are realizations of 2D 'random' ferromagnets. For the collective behavior of such systems, in particular for the 'random ferromagnetic Ising model', considerable temporal stabilities of metastable spin states, characterized by huge magnetic relaxation times and slow domain kinetics, have been reported in literature, see Refs. [27, 120]. Only after extremely long waiting times, the systems may overcome the energy barriers of the rough energy landscape and reach their ferromagnetic equilibrium states. This mechanism also explains the appearance and stability of the nonequilibrium magnetic domain structure of growing films as obtained by our simulations. We conclude that the metastable 'as-grown' domain structure with an intermediate average domain area is caused by the collective behavior of the irregularly coupled island system due to the nonuniform nanostructure.